BA.2.12.1, BA.4 and BA.5 escape antibodies elicited by Omicron BA.1 infection

Xiaoliang Xie (sunneyxie@biopic.pku.edu.cn)
Changping Laboratory https://orcid.org/0000-0001-9281-5239

Yunlong Cao
Peking University https://orcid.org/0000-0001-5918-1078

Ayijiang Yisimayi
Peking University

Fanchong Jian
Peking University https://orcid.org/0000-0001-8703-3507

Weiliang Song
Biomedical Pioneering Innovation Center (BIOPIC), Peking University, Beijing, P.R. China.

Tianhe Xiao
Biomedical Pioneering Innovation Center (BIOPIC), Peking University, Beijing, P.R. China.

Lei Wang
CAS Key Laboratory of Infection and Immunity, National Laboratory of Macromolecules, Institute of Biophysics, Chinese Academy of Sciences, Beijing 100101, China.

Shuo Du
Peking University https://orcid.org/0000-0003-0936-0785

jing wang
https://orcid.org/0000-0002-9084-9985

Qianqian Li
National Institutes for Food and Drug Control

Xiaosu Chen
Institute for Immunology, College of Life Sciences, Nankai University, Tianjin, P. R. China.

Peng Wang
Biomedical Pioneering Innovation Center (BIOPIC), Peking University, Beijing, P.R. China.

Zhiying Zhang
Peking University https://orcid.org/0000-0002-5690-9796

Pulan Liu
School of Life Sciences, Peking University

Ran An
Biomedical Pioneering Innovation Center (BIOPIC), Peking University, Beijing, P.R. China.

Xiaohua Hao
Beijing Ditan Hospital

Yao Wang
Biomedical Pioneering Innovation Center (BIOPIC), Peking University, Beijing, P.R. China.
Jing Wang
Biomedical Pioneering Innovation Center (BIOPIC), Peking University, Beijing, P.R. China.
Rui Feng
Chinese Academy of Sciences
Haiyan Sun
Biomedical Pioneering Innovation Center (BIOPIC), Peking University, Beijing, P.R. China.
Lijuan Zhao
Changping Laboratory
Wen Zhang
Beijing Ditan Hospital, Capital Medical University
Dong Zhao
Beijing Ditan Hospital, Capital Medical University
Jiang Zheng
Changping Laboratory
Lingling Yu
Changping Laboratory
Can Li
Changping Laboratory
Na Zhang
Changping Laboratory
Rui Wang
Changping Laboratory
Xiao Niu
Biomedical Pioneering Innovation Center (BIOPIC), Peking University, Beijing, P.R. China.
Sijie Yang
Biomedical Pioneering Innovation Center (BIOPIC), Peking University, Beijing, P.R. China.
Xuetao Song
Changping Laboratory
Linlin Zheng
Changping Laboratory
Zhiqiang Li
Academy for Advanced Interdisciplinary Studies, Peking University
Qingqing Gu
Changping laboratory
Fei Shao
Biomedical Pioneering Innovation Center (BIOPIC), Peking University, Beijing, P.R. China.
Weijin Huang

NIFDC https://orcid.org/0000-0002-4246-8889

Jin ronghua

https://orcid.org/0000-0001-8496-172X

Zhongyang Shen

Organ Transplant Center, NHC Key Laboratory for Critical Care Medicine, Tianjin First Central Hospital, Nankai University, Tianjin, P. R. China.

Youchun Wang

National Institutes for Food and Drug Control (NIFDC) and WHO Collaborating Center for Standardization and Evaluation of Biologicals, Beijing, China https://orcid.org/0000-0001-9769-5141

Xiangxi Wang

Institute of Biophysics https://orcid.org/0000-0003-0635-278X

Junyu Xiao

Peking University https://orcid.org/0000-0003-1822-1701

Biological Sciences - Article

Keywords:

Posted Date: May 2nd, 2022

DOI: https://doi.org/10.21203/rs.3.rs-1611421/v1

Version of Record: A version of this preprint was published at Nature on June 17th, 2022. See the published version at https://doi.org/10.1038/s41586-022-04980-y.

BA.2.12.1, BA.4 and BA.5 escape antibodies elicited by Omicron infection

Yunlong Cao[1,2,#,*], Ayijiang Yisimayi[2,3,#], Fanchong Jian[2,4,#], Weiliang Song[2,3,#], Tianhe Xiao[2,5,#], Lei Wang[6,#], Shuo Du[3,#], Jing Wang[2,3,#], Qianqian Li[7,#], Xiaosu Chen[8,#], Peng Wang[1], Zhiying Zhang[3], Pulan Liu[3], Ran An[2], Xiaohua Hao[9], Yao Wang[1], Jing Wang[1], Rui Feng[6], Haiyan Sun[1], Lijuan Zhao[1], Wen Zhang[9], Dong Zhao[9], Jiang Zheng[1], Lingling Yu[1], Can Li[1], Na Zhang[1], Rui Wang[1], Xiao Niu[2,4], Sijie Yang[2,10], Xuetao Song[1], Linlin Zheng[1], Zhiqiang Li[10,11], Qingqing Gu[1], Fei Shao[1], Weijin Huang[7], Ronghua Jin[9], Zhongyang Shen[12,*], Youchun Wang[7,*], Xiangxi Wang[6,*], Junyu Xiao[3,10,11,*], Xiaoliang Sunney Xie[1,2,*]

[1]Changping Laboratory, Beijing, P.R. China.

[2]Biomedical Pioneering Innovation Center (BIOPIC), Peking University, Beijing, P.R. China.

[3]School of Life Sciences, Peking University, Beijing, P.R. China.

[4]College of Chemistry and Molecular Engineering, Peking University, Beijing, P.R. China.

[5]Joint Graduate Program of Peking-Tsinghua-NIBS, Academy for Advanced Interdisciplinary Studies, Peking University, Beijing, China.

[6]CAS Key Laboratory of Infection and Immunity, National Laboratory of Macromolecules, Institute of Biophysics, Chinese Academy of Sciences, Beijing, P.R. China.

[7]Division of HIV/AIDS and Sex-transmitted Virus Vaccines, Institute for Biological Product Control, National Institutes for Food and Drug Control (NIFDC), Beijing, P.R. China.

[8]Institute for Immunology, College of Life Sciences, Nankai University, Tianjin, P. R. China.

[9]Beijing Ditan Hospital, Capital Medical University, Beijing, P.R. China.

[10]Peking-Tsinghua Center for Life Sciences, Peking University, Beijing, P.R. China

[11]Academy for Advanced Interdisciplinary Studies, Peking University, Beijing, P.R. China.

[12] Organ Transplant Center, NHC Key Laboratory for Critical Care Medicine, Tianjin First Central Hospital, Nankai University, Tianjin, P. R. China.

[*]Correspondence: Yunlong Cao (yunlongcao@pku.edu.cn); Zhongyang Shen (zhongyangshen@nankai.edu.cn); Youchun Wang (wangyc@nifdc.org.cn); Xiangxi Wang (xiangxi@ibp.ac.cn); Junyu Xiao (junyuxiao@pku.edu.cn); Xiaoliang Sunney Xie (sunneyxie@biopic.pku.edu.cn)

[#]These authors contributed equally.

Abstract

The recently emerged SARS-CoV-2 Omicron sublineages BA.2.12.1, BA.2.13, BA.4 and BA.5 all contain L452 mutations and show potential higher transmissibility over BA.2[1]. The new variants' receptor binding and immune evasion capability require immediate investigation, especially on the role of L452 substitutions. Herein, coupled with structural comparisons, we show that BA.2 sublineages, including BA.2.12.1 and BA.2.13, exhibit increased ACE2-binding affinities compared to BA.1; while BA.4/BA.5 displays the weakest receptor-binding activity due to F486V and R493Q reversion. Importantly, compared to BA.2, BA.2.12.1 and BA.4/BA.5 exhibit stronger neutralization evasion against the plasma of 3-dose vaccinees and, most strikingly, of vaccinated BA.1 convalescents. To delineate the underlying evasion mechanism, we determined the escaping mutation profiles[2], epitope distribution[3] and Omicron sublineage neutralization efficacy of 1640 RBD-directed neutralizing antibodies (NAbs), including 614 isolated from BA.1 convalescents. Interestingly, post-vaccination BA.1 infection mainly recalls wildtype (WT) induced humoral memory and elicits antibodies that neutralize both WT and BA.1. These cross-reactive NAbs are significantly enriched on non-ACE2-competing epitopes; and surprisingly, the majority are undermined by R346 and L452 substitutions, namely R346K (BA.1.1), L452M (BA.2.13), L452Q (BA.2.12.1) and L452R (BA.4/BA.5), suggesting that R346K and L452 mutations appeared under the immune pressure induced by Omicron convalescents. Nevertheless, BA.1 infection can also induce new clones of BA.1-specific antibodies that potently neutralize BA.1 but do not respond to WT SARS-CoV-2 due to the high susceptibility to N501, N440, K417 and E484. However, these NAbs are largely escaped by BA.2 sublineages and BA.4/BA.5 due to D405N and F486V, exhibiting poor neutralization breadths. As for therapeutic NAbs, LY-CoV1404 (Bebtelovimab[4]) and COV2-2130 (Cilgavimab[5]) can still effectively neutralize BA.2.12.1 and BA.4/BA.5, while the S371F, D405N and R408S mutations carried by BA.2/BA.4/BA.5 sublineages would undermine most broad sarbecovirus NAbs. Together, our results indicate that Omicron can evolve mutations to specifically evade humoral immunity elicited by BA.1 infection. The continuous evolution of Omicron poses great challenges to SARS-CoV-2 herd immunity and suggests that BA.1-derived vaccine boosters may not be ideal for achieving broad-spectrum protection.

Main

The recent emergence and global spreading of severe acute respiratory syndrome coronavirus 2 (SARS-CoV-2) variant Omicron (B.1.1.529) have posed a critical challenge to the efficacy of COVID-19 vaccines and neutralizing antibody therapeutic[6-8]. Due to multiple mutations to the spike protein, including its receptor-binding domain (RBD) and N-terminal domain (NTD), Omicron can cause severe neutralizing antibody evasion[3,9-12]. Currently, Omicron sublineage BA.2 has rapidly surged worldwide, out-competing BA.1 and accounting for over 95% of recent COVID-19 cases. Compared to the RBD of BA.1, BA.2 contains three additional mutations, including T376A, D405N and R408S, and lacks the G446S and G496S harbored by BA.1 (Extended Data Fig. 1a). The S371L on BA.1 is also substituted with S371F in BA.2. These differences between BA.1 and BA.2 on the RBD can lead to their different resistance to multiple therapeutic antibodies[13]. Importantly, new Omicron variants are still continuously emerging. The recently appeared new variants contain identical RBD sequences to BA.2 with the addition of L452 and F486 substitutions, namely BA.2.12.1 (L452Q), BA.2.13 (L452M), BA.4 and BA.5 (L452R+F486V), and displayed higher transmission advantage over BA.2. BA.2.12.1 already appears to be near 30% of the total new infections in the United States. BA.2.13 contributes 5% of new sequences in Belgium, while BA.4 and BA.5 together account for 50% of new sequences in South Africa. The new variants' receptor binding and immune evasion capability require immediate investigation, especially on the role of L452 substitutions.

Structural analyses of Omicron Spike

To systematically compare the structural and functional properties of the Omicron subvariants, we first expressed and purified the prefusion-stabilized trimeric ectodomains of BA.1, BA.2, BA.3, BA.2.12.1, BA.2.13 and BA.4/BA.5 Spike (S-trimer). Noteworthy, BA.4 and BA.5 share the same spike mutations. All spike-trimers contain GSAS and 6P mutations along with the T4 fibritin trimerization domain[14,15]. We determined the cryo-EM reconstructions of these S-trimers at an overall resolution of 3.1-3.5 Å, together with our previous reported BA.1 structure, allowing us to

compare the detailed structural variations across Omicron sublineages (Fig. 1a and Extended Data Fig. 1b). Distinct from stably maintaining an open conformation for receptor recognition with one 'up' RBD and two 'down' RBDs observed in BA.1 S-trimer [16], BA.2 and BA.2.12.1 exhibit two conformational states corresponding to a closed-form with all three RBDs "down" and an open form with one RBD "up". Notably, one RBD was clearly disordered, representing a stochastic movement in BA.2.13, which, together with BA.2 and BA.2.12.1, suggests structural heterogeneity in the S-trimers of BA.2 sublineages. Surprisingly, most BA.3 and BA.4 S-trimers adopt closed- or semi-closed forms (Fig. 1a), similar to structural observations of HKU1 and HCoV-NL63, which may correlate with decreased infectivity and fitness in humans. Interestingly, BA.2 sublineage S-trimers harbor relatively less compacted architectures in the region formed by the three copies of S2 (Fig. 1b). By contrast, BA.1, BA.3 and BA.4 possess relatively tight inter-subunit organization with the more buried areas between S2 subunits (Fig. 1b). In line with structural observations, thermal stability assays also verified that S-trimers from BA.2 sublineages were the least stable among these variants, which might confer enhanced fusion efficiencies (Fig. 1c).

ACE2-binding comparison of Omicron Spike

We measured the binding affinity between hACE2 and S-trimers of the Omicron variants by surface plasmon resonance (SPR) (Fig. 1d). BA.2 sublineages exhibited further improved binding activities to hACE2, while BA.4 showed a substantially decreased binding affinity. The affinity of BA.3 to hACE2 is largely maintained compared to that of BA.1 (Fig. 1d). Structural comparisons revealed that the lack of G496S in BA.2 sublineages compared to BA.1 and BA.3 retained the hydrogen bond with K353 to hACE2, increasing their binding capability, which is in line with experimental observations revealed by deep mutational scanning assay[17]. Unexpectedly, a local conformational perturbation surrounding residues 444-448 lost its hydrophilic interaction between S446 with Q42 from hACE2 in BA.3, which is presumably caused by the single mutation G446S rather than double mutations of G446S and G496S (Fig. 1e). Remarkably, BA.4 substantially decreased its binding activity due to reduced hydrophobic and hydrophilic

interactions caused by substitutions of F486V and R493Q, respectively (Fig. 1e). Together, BA.2 sublineages, including BA.2.12.1 and BA.2.13, exhibit higher ACE2 binding affinities and lower S-trimer stability than other Omicron variants. Contrarily, BA.4 and BA.5 displayed decreased receptor binding capabilities, which may hinder the speed of their spreading.

Plasma evasion of BA.2.12.1, BA.2.13 and BA.4/5

To probe the neutralization evasion ability of the recently emerged Omicron sublineages, we first performed pseudovirus neutralization assays using D614G and Omicron sub-variants, including BA.1, BA.1.1, BA.2, BA.3, BA.2.12.1, BA.2.13, BA.4/BA.5, against the plasma obtained from 3-dose vaccinated individuals, BA.1 convalescents, and vaccinated SARS convalescents (Supplementary Table 1). Plasma samples were collected 4 weeks after the booster shot or 4 weeks after COVID-19 hospital discharge. In vaccine-boosted individuals, BA.1, BA.1.1 and BA.2 showed no significant difference in plasma neutralization resistance (Fig. 2a-b), which is concordant with previous reports[18,19]. However, we found that BA.2 sub-variants BA.2.13 and BA.2.12.1 showed increased immune evasion capability than BA.2, with BA.2.12.1 stronger than BA.2.13; while BA.4/BA.5 confers even stronger antibody escape (Fig. 2a-b). The drop in neutralization efficacy is more severe in the plasma obtained from individuals infected by BA.1 who had received 3-dose CoronaVac before infection (Fig. 2c). The plasma NT50 of BA.1 convalescents against BA.2.13, BA.2.12.1 and BA.4/5, compared to that against BA.1, was reduced by 2.0x, 3.7x and 8.0x fold, respectively. Interestingly, plasma from vaccinated SARS convalescents showed a different phenotype than normal vaccinees, such that BA.2 sub-variants and BA.3/BA.4/BA.5 could cause a striking neutralization loss (Fig. 2d). This suggests that certain BA.2 mutations may specifically evade broad sarbecovirus neutralizing antibodies which are substantially enriched in vaccinated SARS convalescents[20]. Together, these observations indicate that the newly emerged BA.2.13, BA.2.12.1 and BA.4/5 display stronger and distinct humoral immune evasion than BA.1 and BA.2.

Next, we examined the reaction difference in neutralizing activities of therapeutic antibodies

against Omicron subvariants (Fig. 2e). All of the seven Omicron subvariants displayed striking evasion against neutralization by Class 1 and 2 RBD antibodies, such that REGN-10933[21], LY-CoV016[22] and LY-CoV555[23], COV2-2196[5] and BRII-196[24] were strongly affected, while DXP-604[15,25] were evaded only by BA.4/5, showing reduced but still competitive efficacy against BA.1 and BA.2 subvariants. This is understandable since Omicron subvariants share most mutations in the receptor-binding motif (Extended Data Fig. 1a). Two major antigenicity differences were observed between BA.1 and BA.2 subvariants. First, neutralizing antibodies targeting the linear epitope 440-449[3], such as REGN-10987[21] and COV2-2130[5], retained neutralizing potency against BA.2 subvariants and BA.4/5. Second, BA.2 escapes or greatly reduces the efficacy of BA.1 effective broad sarbecovirus neutralizing antibodies, including ADG-2[26] and S309[27]. The ACE2-mimicking antibody S2K146[28] could potently neutralize all BA.1 and BA.2 subvariants but showed reduced activity against BA.4/5, similar to DXP-604. BRII-196 and BRII-198 cocktail were escaped by BA.2 sublineages and BA.3/BA.4/BA.5. Notably, LY-CoV1404[29] demonstrated high potency against all assayed Omicron subvariants, and COV2-2130 can potently neutralize emerging BA.2 subvariants and BA.4/5. In addition, our recently developed antibody cocktail isolated from vaccinated SARS convalescents, namely SA58 (BD55-5840, Class 3) and SA55 (BD55-5514, Class 1/4), displayed high potency against all Omicron variants and sarbecoviruses SARS-CoV-1, Pangolin-GD and RaTG13.

NAb repertoire of BA.1 breakthrough infection

To delineate the underlying antibody evasion mechanism of BA.2.13, BA.2.12.1 and BA.4/BA.5, especially on how they escape the humoral immunity induced by BA.1 convalescents and vaccinated SARS convalescents, we started by isolating RBD-targeting NAbs from those individuals (Extended Data Fig. 2a)[25,30]. First, antigen-specific memory B cells were isolated by fluorescence-activated cell sorting (FACS) from pooled PBMCs using double RBD^{WT}+ selection for 3-dose vaccinees, RBD^{WT}+ RBD^{SARS}+ selection for vaccinated SARS convalescents and double $RBD^{BA.1}$+ selection for BA.1 convalescents (Extended Data Fig. 2b). Secondly, we

performed single-cell V(D)J sequencing (scVDJ-seq) with $RBD^{BA.1}$ and RBD^{WT} feature barcodes to the $CD27^{+}/IgM^{-}$ antigen-specific memory B cells (Extended Data Fig. 2b). Thirdly, we extracted the productive heavy-light chain paired VDJ sequences and expressed the antibodies *in vitro* as human IgG1. Interestingly, during this process, we found that the majority of Omicron-reactive memory B cells from BA.1 convalescents who received 3-dose CornonaVac could also bind to WT RBD (Fig. 2f). In contrast, only around one-fourth of Omicron-reactive memory B cells isolated from unvaccinated BA.1 convalescents could bind to WT RBD (Fig. 2f). Also, the bivalent antigen-binding property could only be observed in IgM-CD27+ memory B cells, but not IgM+CD27- naïve B cells (Fig. 2g). In addition, ~80% of the sequenced $BA.1^{+}$ cells were BA.1/WT bivalent, determined by the detected number of BA.1 RBD and WT RBD feature barcodes (Fig. 2h). VDJ sequence analysis revealed significantly higher heavy chain V-domain somatic hypermutation (SHM) rates of BA.1/WT bivalent B cell receptors (BCRs) than that of BA.1-specific BCRs (Fig. 2i), which implies bivalent memory B cells were further affinity-matured compared to BA.1-specific memory B cells. Together, these suggest that post-vaccination infection with Omicron BA.1 mainly recalls WT-induced memory B cells, supporting the "original antigenic sin" theory.

To further specify the epitope distribution of NAbs elicited by post-vaccination BA.1 infection, we applied high-throughput yeast-display-based deep mutational scanning (DMS) assays[2,3] that cover all possible single residue substitutions in WT RBD background, and successfully determined the escaping mutation profiles of 1640 RBD-binding antibodies. Among these antibodies, 602 were from SARS-CoV-2 WT convalescents or 3-dose vaccinees, 614 from post-vaccination BA.1 convalescents, and 410 SARS/WT cross-reactive antibodies from vaccinated SARS convalescents (Supplementary Table 2). 14 antibodies with published DMS profiles are also included [2,31,32]. It is important to note that, among the 614 antibodies from post-vaccination BA.1 convalescents, 102 are BA.1-specific and do not bind to WT RBD, where we applied Omicron BA.1-based DMS. The remaining 1538 RBD^{WT}-reactive antibodies were unsupervised clustered into 12 epitope groups according to their WT-based mutational escaping profiles using t-

distributed stochastic neighbor embedding (t-SNE) (Fig. 3a), adding 6 more epitope groups compared to our previous classification[3].

Group A-C recapitulates our previous taxonomy[3], in which the members mainly target the ACE2-binding motif[33-37] (Extended Data Fig. 3a). Group D antibodies, such as REGN10987, LY-CoV1404 and COV2-2130, bind to the linear epitope 440-449 on the RBD and are expanded into D1 and D2 subgroups. Group D1 is more affected by R346 and L452, while D2 antibodies do not (Extended Data Fig. 3b). Additionally, Group E and F are now expanded into E1-E3 and F1-F3, which covers the front and backside of RBD, roughly corresponding to Class 3 and Class 4, respectively[36] (Extended Data Fig. 3a). Group E1 corresponds to the S309 binding site, whose epitope involves G339 and R346 (Extended Data Fig. 3b). Group E2 antibodies bind to the front chest of RBD[34] and do not compete with ACE2 (Fig. 3d), where E2.1 is more affected by R346 and A348, while E2.2 is more affected by R357 (Extended Data Fig. 3a-c). Group E3 (S2H97 site) and F1 (S304 site) bind to highly conserved regions on the bottom of RBD, mainly contacting with K462/S514/E516, and S383/T385/K386, respectively (Extended Data Fig. 3c). Group E1-E3 and F1 antibodies do not compete with ACE2, while F2 and F3 antibodies are ACE2-competing and affected by T376, K378, D405, R408 and G504 (Fig. 3d and Extended Data Fig. 3b-c), corresponding to Class 1/4[38].

Pseudovirus neutralizing efficacy of antibodies in each group against SARS-CoV-1, SARS-CoV-2 D614G, Pangolin-GD and RaTG13 is tested, and their binding capability to 22 sarbecovirus RBDs is measured through ELISA (Supplementary Table 2 and Supplementary Table 3). We found that antibodies of the same cluster have unified sarbecovirus neutralization potency and binding spectra (Fig. 3e, Extended Data Fig. 4). In total, five clusters of antibodies exhibiting broad sarbecovirus binding ability were identified, namely Groups E1, E3, F1, F2 and F3 (Extended Data Fig. 4), of which E1, F2 and F3 showed potent neutralizing activity against SARS-CoV-1 (Fig.3e).

We found that compared to WT convalescents or vaccinees, the plasma of vaccinated SARS convalescents enriched Group E1, E3, F1, F2 and F3 antibodies, which bind conserved epitopes among sarbecoviruses and display broad sarbecovirus neutralizing activity (Fig. 3b-c). However, revealed by DMS, we know that F2 and F3 antibodies are susceptible to D405N and R408S mutations (Extended Data Fig. 3b), and BA.2 sublineages and BA.3/BA.4/BA.5 may dampen those NAbs, explaining the sharp drop of plasma NT50 against Omicron variants other than BA.1 sublineages (Fig. 2d). Importantly, we also found that the humoral immunity elicited by post-vaccination BA.1 infection enriched Group E2.1, E2.2 and F1 antibodies (Fig. 3b-c), which do not compete with ACE2 (Fig. 3d). Though not enriched, the ACE2-competing Group B and D1 antibodies remain highly abundant. Since E2, D1 and B antibodies are sensitive to 452 and 486 mutations (Extended Data Fig. 3b), it is highly possible that the newly emerged BA.2.12.1, BA.2.13, BA.4/BA.5 can specifically target those antibodies, rationalizing the huge loss in plasma NT50 against those variants (Fig. 2c).

NAb evasion of BA.2.12.1, BA.2.13 and BA.4/5

To examine our hypothesis, we measured pseudovirus neutralization of those NAbs against BA.2.12.1, BA.2.13 and BA.4/BA.5, as well as the major Omicron variants BA.1, BA.1.1, BA.2 and BA.3 (Fig. 3f). Interestingly, NAbs from different epitope groups displayed distinct neutralizing activities against Omicron variants. Also, BA.1-stimulated antibodies (from BA.1 convalescents) and WT-stimulated (from WT convalescents or vaccinees, with or without previous SARS-CoV-1 infection) showed significantly higher potency and breadth in most epitope groups, suggesting a higher affinity maturation (Fig. 3f).

Most WT-stimulated Group A, B and C antibodies were largely escaped by Omicron variants, while a subset showed broad Omicron effectiveness (Fig. 3f). These antibodies are largely enriched in BA.1-stimulated groups and generally use similar heavy chain V genes compared to WT-stimulated antibodies, but display higher convergence (Extended Data Fig. 5a-b). These broad NAbs in groups A, B and C are also shown to be enriched in individuals who received a booster

dose of mRNA vaccines[38], which probably accounts for the high plasma neutralizing activity of 3-dose mRNA vaccinees against Omicron variants. Nevertheless, BA.1-stimulated groups B and C NAbs were significantly evaded by BA.4 due to F486V and L452R, concordant with results from DMS (Extended Data Fig. 6a-b).

Group D antibodies are most affected by G446S in BA.1, BA.1.1 and BA.3; thus, these NAbs showed higher potency against BA.2 (Fig. 4a-b). However, D1 antibodies showed reduced efficacy against L452 substitutions, with L452M (BA.2.13) causing mild escapes, L452Q causing moderate escapes (BA.2.12.1), and L452R (BA.4/BA.5) causing severe escapes (Fig. 4c-d). In contrast, D2 antibodies, especially those stimulated by BA.1 infection, showed exceptional broad and potent neutralizing activity against all Omicron subvariants, such as Ly-CoV1404 (Fig. 4b and Extended Data Fig. 7a). However, the linear epitope of these antibodies is not conserved (Fig. 4d), suggesting that their good breadth is possibly due to their rarity in WT and BA.1 convalescents (Fig. 3b).

E2 antibodies bind to the chest of RBD[34] (Fig. 4a), and their epitopes focus around R346, A348, A352, K356, R357 and I468 (Fig. 4d). Despite similar epitopes, E2.1 antibodies, especially those BA.1-stimulated, display significantly higher neutralizing potency than E2.2 (Fig. 4b and Extended Data Fig. 8a-b). Interestingly, L452 substitutions also cause large-scale escapes of E2.1 and E2.2 antibodies (Fig. 4c). Similar to the D1 epitope group, L452R and L452Q cause much stronger antibody evasion than L452M (Fig. 4c). Noteworthy, DMS does not reveal the L452 sensitivities of the E2.2 epitope group (Fig. 4d). Together, our results suggest that Omicron evolved mutations at L452, especially L452Q and L452R, to specifically evade NAbs from D1 and E2, consequently maximizing Omicron convalescents' humoral immune evasion. Importantly, D1 and E2.1 antibodies also showed decreased efficacy against BA.1.1 compared to BA.1 due to R346K, since both epitope groups are sensitive to R346K substitutions (Fig. 4b), which shed lights on the prevalence of BA.1.1 over BA.1 in the United States.

BA.2 escapes broad sarbecovirus NAbs

In total, five clusters of antibodies were found to exhibit broad sarbecovirus neutralizing ability with diverse breadth, namely Group E1, E3, F1, F2 and F3 (Fig, 3e and Extended Data Fig. 4). However, we found that BA.1-effective E1, F2 and F3 NAbs displayed a systematic reduction in neutralization activity against BA.2 subvariants and BA.3/BA.4/BA.5 (Fig. 2e and 5a-c), while Group E3 and F1 antibodies demonstrated weak neutralizing activity against all variants (Fig. 3f and Extended Data Fig. 8a) due to their highly conserved binding sites (Extended Data Fig. 8b-c). The mechanisms behind the neutralization loss of those broad sarbecovirus antibodies are unclear and require investigation, which is critical for developing broad-spectrum sarbecovirus vaccines and antibody therapeutics.

To study why BA.2 subvariants and BA.3/BA.4/BA.5 could systematically reduce the neutralization efficacy of E1 antibodies, we solved the cryo-EM structures of two BA.1 neutralizing E1 antibodies, BD55-3152 and BD55-5840 (SA58), in complex with BA.1 spike proteins using cryo-electron microscopy (cryo-EM) (Fig. 5f, Extended Data Fig. 9a and 9c). Like S309, E1 antibodies' epitope involves an N-linked glycan on N343 (Fig. 5f). Besides, members of Group E1 are generally sensitive to the changes of G339, E340, T345 and especially R346, revealed by their escaping mutation profiles (Fig. 5e). Intriguingly, the newly acquired mutations of BA.2 do not overlap with the shared epitope of E1 antibodies, suggesting that the systematic reduction of neutralization is not caused by amino-acid substitution, but potentially due to structural alteration. To explore this hypothesis, we further determined the cryo-EM structure of the prefusion-stabilized BA.2 spike in complex with the BD55-5840 Fab (Fig. 5g). A structural comparison with the BA.1 RBD binding to BD55-5840 described above suggests that the 366-377 hairpin loop displays significant conformational differences due to S371F and T376A mutations (Fig. 5g). As a result, the bulky Phe resulting from the S371F mutation interferes with the positioning of the glycan moiety attached to N343, which in turn budges the heavy chain of BD55-5840 upward. This may explain the reduction of the binding of BD55-5840 and S309, rationalizing their reduced neutralizing activity (Fig. 5a and Extended Data Fig. 9b). Importantly, the N343 glycan is critically recognized by almost all E1 neutralizing antibodies, including S309. Thus, this

group of broad and potent neutralizing antibodies is likely affected by the S371F mutation in a systematic manner through N343-glycan displacement.

The epitopes of group F2 and F3 antibodies cover a continuous surface on the backside of RBD and can only bind to the up RBDs (Fig. 2b). To probe how BA.2 escapes antibodies of group F2 and F3, we solved the cryo-EM structure of two representative BA.1-effective antibodies in these groups, BD55-1239 from group F2, and BD55-3372 from group F3, in complex with the BA.1 and Delta spike protein respectively (Fig. 5h-i and Extended Data Fig. 9a). Group F2 antibodies can be escaped by RBD mutation involving T376, K378, and R408 (Fig. 5e). Indeed, these residues are all at the heart of BD55-1239's epitope, and are fairly conserved across sarbecoviruses (Fig. 5e). Importantly, D405N and R408S harbored by Omicron BA.2 sublineages could alter the antigenic surface that disrupts the binding of F2 antibodies (Fig. 5i), hence completely abolishing the neutralizing capacity of F2 antibodies (Fig. 5b). Similarly, the D405N and R408S mutations harbored by BA.2 subvariants could interrupt the heavy-chain binding of F3 antibodies, causing large-scale escapes of BA.1-effective F3 neutralizing antibodies (Fig. 5c and 5i). The above observations were further validated by neutralizing activity against spike-pseudotyped VSV harboring D614G+D405N and D614G+R408S. As expected, Group E1 antibodies were affected by neither D405N nor R408S single substitution, while F2 and F3 antibodies displayed significantly decreased activity (Fig. 5d). Nevertheless, several members of F3 antibodies are not sensitive to the D405N and R408S mutations of BA.2, making them good therapeutic drug candidates, such as BD55-5514 (SA55) (Fig. 2e). In sum, we revealed that S371F, D405N and R408S mutations harbored by BA.2 and emerging Omicron variants could induce large-scale escapes of broad sarbecovirus neutralizing antibodies, which is critical to the development of broad sarbecovirus antibody therapeutics and vaccines.

BA.1-specific NAbs exhibit poor breadths

Besides all those NAbs that could bind to WT, it is also important to investigate the epitope distribution of BA.1-specific NAbs that do not react with WT RBD. To do so, we built the yeast display variants library based on RBD BA.1, and determined the escape mutation maps of 102 BA.1-specific antibodies. By integrating analysis of the whole dataset containing 1640 SARS-CoV-2 RBD antibodies, we got the embedded features of the BA.1-specific NAbs and performed clustering and t-SNE similarly. The 102 NAbs were clustered into four BA.1-specific epitope groups, named A^{Omi}, B^{Omi}, D^{Omi}, and $F3^{Omi}$ (Fig. 6a), because these groups are highly related to their corresponding WT epitope groups (Fig. 6d). These antibodies are all ACE2-competing and cannot neutralize D614G and SARS-CoV-1 (Fig. 6b), probably due to N417K/Y501N/H505Y for A^{Omi}, A484E/K478T for B^{Omi}, K440N for D^{Omi}, and R498Q/Y501N for $F3^{Omi}$, as indicated by average escape maps of each group (Fig. 4c). Nearly all of the BA.1-specific NAbs showed poor cross-reactivity among Omicron subvariants. Specifically, most antibodies in $F3^{Omi}/A^{Omi}$ are evaded by BA.2 subvariants and BA.3 possibly due to D405N, and antibodies in B^{Omi} are strongly escaped by BA.4 due to F486V. Some D^{Omi} antibodies might be affected with S446G and were evaded by BA.2 subvariants and BA.4, which were not captured by DMS (Fig. 5b-c and Extended Data Fig. 10b). Only a small group of D^{Omi} antibodies displayed cross-reactivity among all Omicron subvariants. Interestingly, these BA.1-specific NAbs displayed different heavy chain V gene usage compared to WT-reactive antibodies in the corresponding epitope group. Specifically, antibodies in A^{Omi} and B^{Omi} did not show significant convergence. IGHV3-53/3-66 only contributes to a small subset of A^{Omi} antibodies. Instead, D^{Omi} antibodies were dominant by IGHV2-70 and IGHV5-51, while IGHV4-59 for F^{Omi} (Extended Data Fig. 10a). These three V genes also appeared in WT-reactive antibodies, but were relatively rare and did not show significant epitope enrichment (Extended Data Fig. 5a-b).

In this study, we showed that Omicron is continuously evolving under immune pressure, and rationalized the appearance of R346K (BA.1.1) and L452 substitutions. Unlike when Omicron first appeared, now Omicron sublineages have started to target the humoral immunity induced by Omicron itself, including the humoral immunity induced by post-vaccination Omicron infection.

This poses a great challenge to the currently established herd immunity through WT-based vaccination and BA.1/BA.2 infection. Similarly, this observation also suggests that Omicron BA.1-based vaccine may not be the ideal antigen for inducing broad-spectrum protection against emerging Omicron sublineages.

Here, by combining high-throughput single-cell sequencing and high-throughput yeast display-based deep mutational screening, we showcased the ability to decipher the complicated humoral immune repertoire elicited by Omicron infection and the underlying immune evasion mechanism of L452 mutations. The alibility to dissect the entire humoral immunity into distinct antibody epitope groups greatly increase the resolution of antibody and mutational escape research. As we have shown, the antibodies in each epitope group show highly concordant attributes and features, largely facilitating the investigation of the immune evasion mechanism of circulating variants. The comprehensive data we provided in this research gives critical instructions to the development of broad-spectrum sarbecovirus vaccines and therapeutic antibodies.

Figure 1

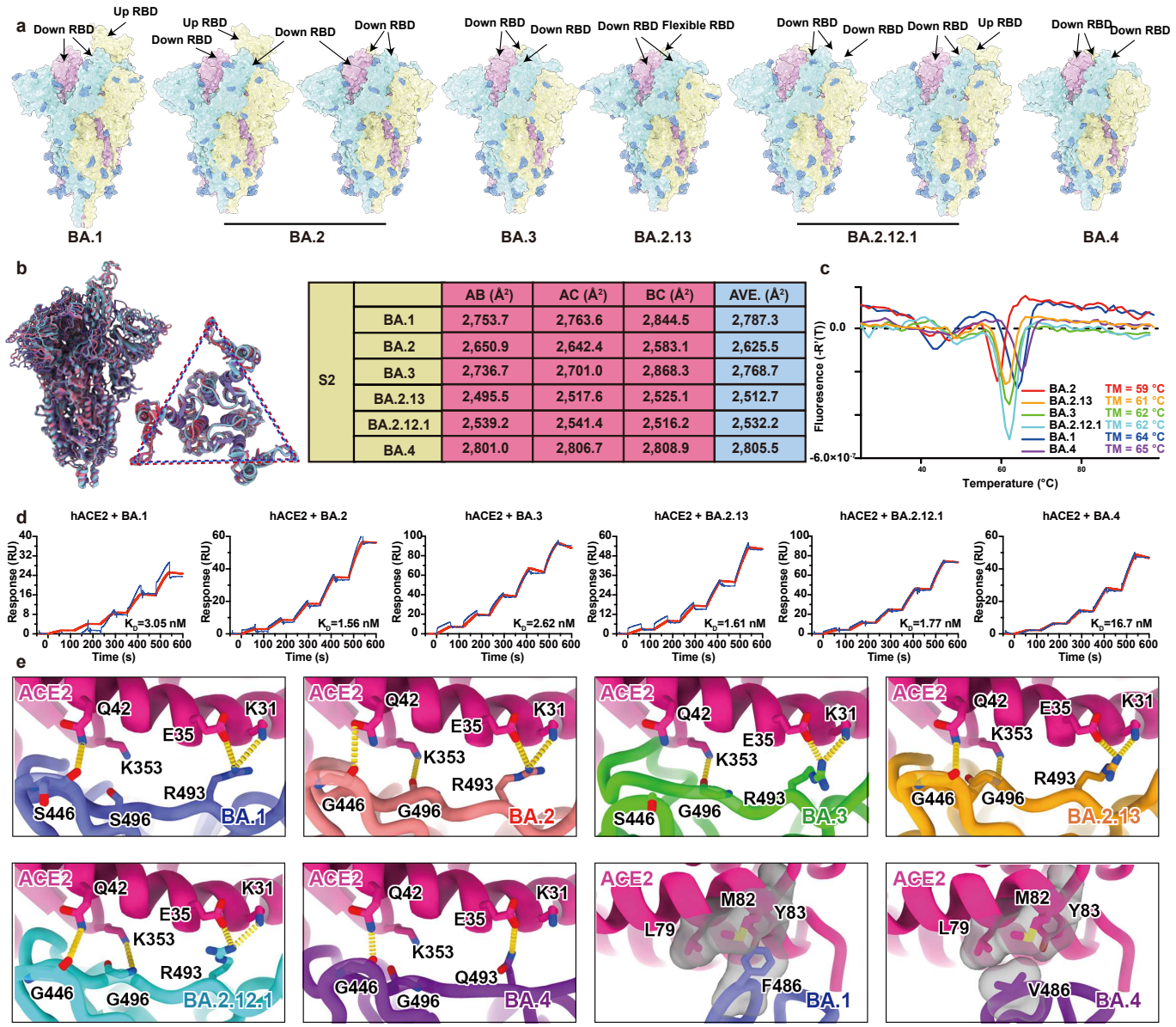

Fig. 1 | Structural characteristics of Omicron subvariants

a, Surface representation for structures of S trimer of BA.1, BA.2, BA.3, BA.2.13, BA.2.12.1 and BA.4 variants. b, Structural interpretation and functional verification for the stability of S protein for BA.1, BA.2, BA.3, BA.2.13, BA.2.12.1 and BA.4 variants. The superimposed structures for S protein and the S2 domains of BA.1 (purple), BA.2 (red) and BA.4 (blue) are shown on the left. The binding surface areas between S2 subunits of all variants are calculated in the table on the right. c, Thermoflour analysis for these Omicron variants. Curves for each Omicron variant are colored in rainbow (BA.1: blue; BA.2: red; BA.3: green; BA.2.13: orange; BA.2.12.1: cyan; BA.4: purple). d, Binding affinities of S-trimers of Omicron variants to hACE2 measured by SPR. e, Details of interactions between hACE2 and RBD of Omicron variants. Structures of the RBD from Omicron variants and hACE2 are shown as ribbons. Color scheme is same as b.

Figure 2

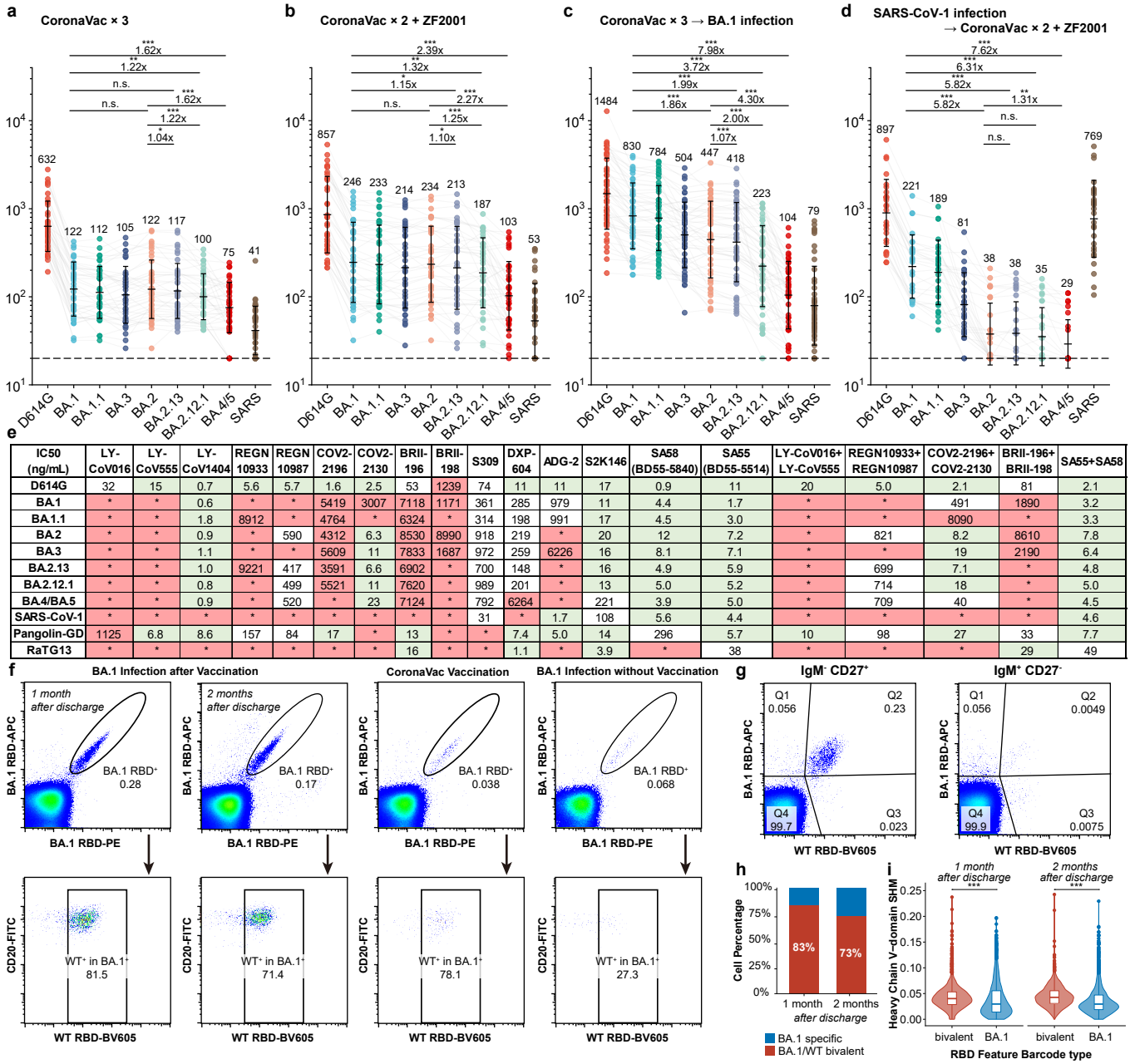

IC50 (ng/mL)	LY-CoV016	LY-CoV555	LY-CoV1404	REGN 10933	REGN 10987	COV2-2196	COV2-2130	BRII-196	BRII-198	S309	DXP-604	ADG-2	S2K146	SA58 (BD55-5840)	SA55 (BD55-5514)	LY-CoV016+ LY-CoV555	REGN10933+ REGN10987	COV2-2196+ COV2-2130	BRII-196+ BRII-198	SA55+SA58
D614G	32	15	0.7	5.6	5.7	1.6	2.5	53	1239	74	11	11	17	0.9	11	20	5.0	2.1	81	2.1
BA.1	*	*	0.6	*	*	5419	3007	7118	1171	361	285	979	11	4.4	1.7	*	*	491	1890	3.2
BA.1.1	*	*	1.8	8912	*	4764	*	6324	*	314	198	991	17	4.5	3.0	*	*	8090	*	3.3
BA.2	*	*	0.9	*	590	4312	6.3	8530	8990	918	219	*	20	12	7.2	*	821	8.2	8610	7.8
BA.3	*	*	1.1	*	*	5609	11	7833	1687	972	259	6226	16	8.1	7.1	*	*	19	2190	6.4
BA.2.13	*	*	1.0	9221	417	3591	6.6	6902	*	700	148	*	16	4.9	5.9	*	699	7.1	*	4.8
BA.2.12.1	*	*	0.8	*	499	5521	11	7620	*	989	201	*	13	5.0	5.2	*	714	18	*	5.0
BA.4/BA.5	*	*	0.9	*	520	*	23	7124	*	792	6264	*	221	3.9	5.0	*	709	40	*	4.5
SARS-CoV-1	*	*	*	*	*	*	*	*	*	31	*	1.7	108	5.6	4.4	*	*	*	*	4.6
Pangolin-GD	1125	6.8	8.6	157	84	17	*	13	*	*	7.4	5.0	14	296	5.7	10	98	27	33	7.7
RaTG13	*	*	*	*	*	*	*	16	*	*	1.1	*	3.9	*	38	*	*	*	29	49

Fig. 2 | BA.2.12.1, BA.4 and BA.5 exhibit stronger antibody evasion than BA.2.

a-d, Neutralizing titers against SARS-CoV-2 D614G, Omicron subvariants and SARS-CoV-1 pseudoviruses in plasma from vaccinated and convalescent individuals. a, Individuals who received 3 doses of CoronaVac (n=40). b, Individuals who received 2 doses of CoronaVac and 1 dose of ZF2001 (n=38). c, BA.1 convalescents who had received 3 doses of CoronaVac before infection (n=50). d, SARS convalescents who received 2 doses of CoronaVac and 1 dose of ZF2001 (n=28). P-values were calculated using a two-tailed Wilcoxon signed-rank test, in comparison to IC50 against BA.2. *, <0.05; **, <0.01; ***, <0.001; n.s., not significant. e, Neutralizing activity against SARS-CoV-2 variants and sarbecoviruses by therapeutic neutralizing antibodies. green, IC50 < 30ng/mL; red, IC50 > 1,000ng/mL; *, IC50 > 10,000ng/mL. f, FACS analysis of pooled memory B cells (IgM-/ CD27+) from BA.1 breakthrough infection convalescents, vaccinated individuals, and BA.1 convalescents without vaccination. g, Antigen binding status of B cells (CD20+) from BA.1 convalescents who received 3 dose CoronaVac. Left, memory B cells (IgM-/ CD27+); right, naïve B cells (IgM+/ CD27-). h, The ratio of RBD^{WT} and $RBD^{BA.1}$ feature barcodes detected by 10x single-cell VDJ sequencing of BA.1 binding memory B-cells elicited by post-vaccination BA.1 infection convalescents. i, Heavy chain V-domain somatic hypermutation (SHM) rate of BA.1-specific and BA.1/WT bivalent BCRs in post-vaccination BA.1 infection convalescents. All neutralization assays were conducted in biological duplicates.

Figure 3

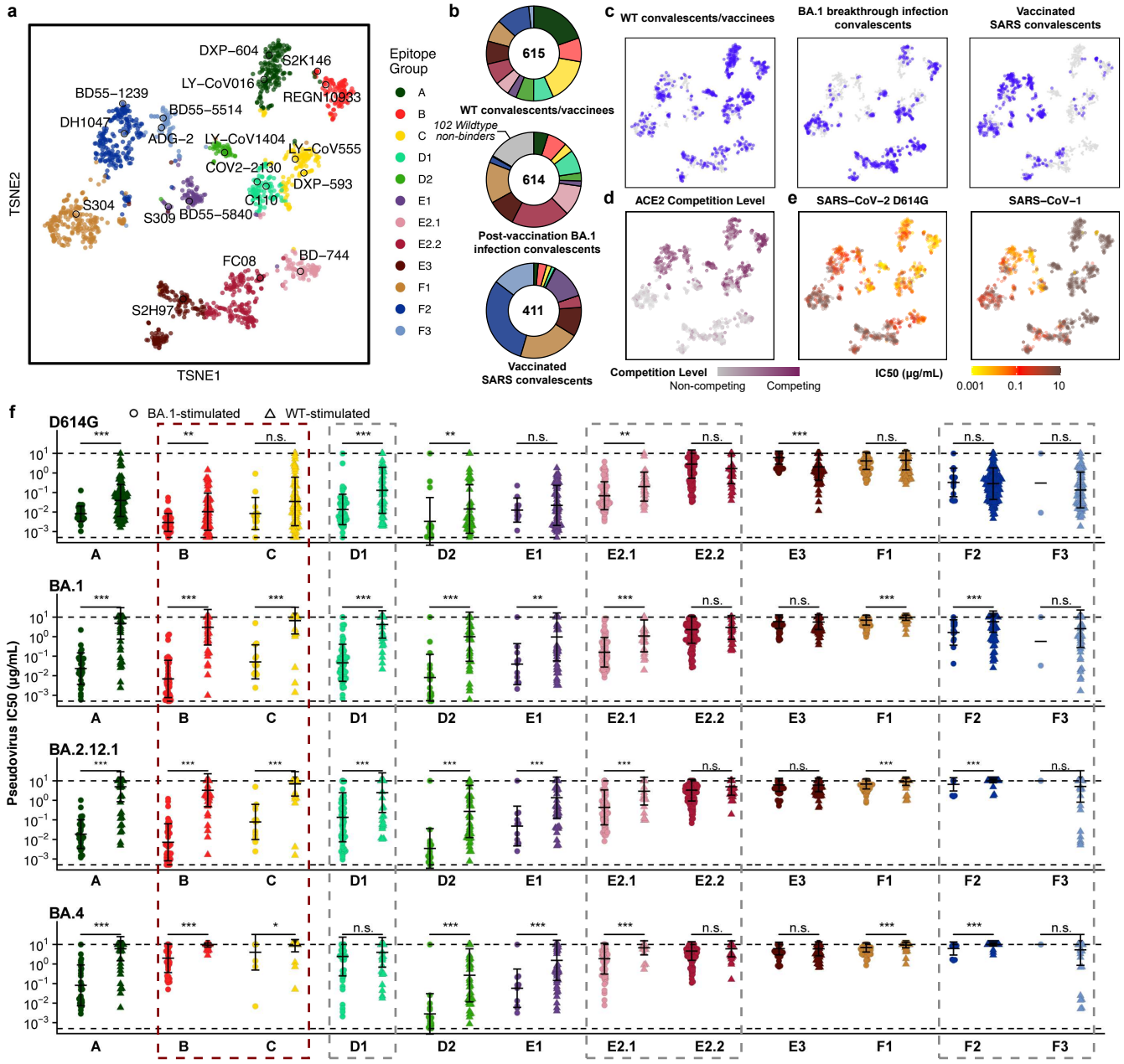

Fig. 3 | Comprehensive epitope mapping and neutralization analyses of SARS-CoV-2 RBD antibodies. a, t-SNE and unsupervised clustering of SARS-CoV-2 wildtype RBD-binding antibodies. 12 epitope groups were identified based on deep mutational scanning of 1538 antibodies. b-c, Epitope distribution of 615 antibodies from wildtype convalescents, 512 antibodies from post-vaccination BA.1 infection convalescents, and 411 vaccinated SARS convalescents. A panel of 102 BA.1-specific antibodies that do not bind wildtype were also isolated from BA.1 convalescents. d, ACE2 competition level determined by competition ELISA (n=1286) were projected onto the t-SNE. e, Neutralizing activity against SARS-CoV-2 D614G (n=1509) and SARS-CoV-1 (HKU-39849, n=1457), respectively. f, Neutralizing activity against SARS-CoV-2 D614G and Omicron subvariants pseudovirus by antibodies of each epitope group from BA.1 convalescents (BA.1-stimulated), and from wildtype convalescents or vaccinees (WT-stimulated, including SARS convalescents). P-values were calculated using a two-tailed Wilcoxon rank-sum test, in comparison to IC50 against BA.2. *, <0.05; **, <0.01; ***, <0.001; n.s., not significant.

Figure 4

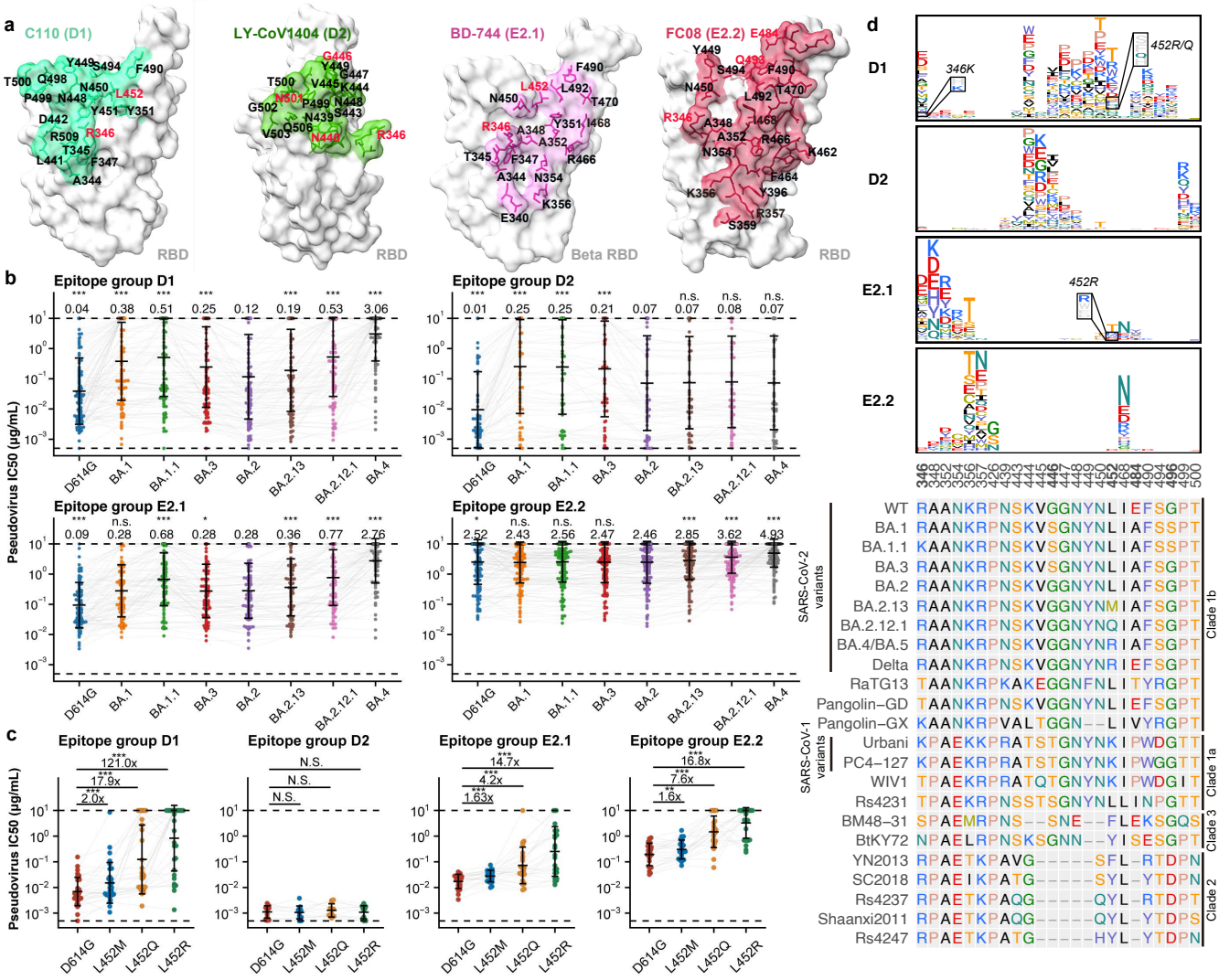

Fig. 4 | Bivalent neutralizing antibodies elicited by BA.1 were evaded by L452 mutations

a, Epitope of representative antibodies in group D1 (C110, PDB: 7K8V), D2 (LY-CoV1404, PDB: 7MMO), E2.1 (BD-744, PDB: 7EY0), and E2.2 (FC08, PDB: 7DX4). Residues highlighted in red indicate mutated sites in Omicron variants. b, Neutralizing activity of antibodies in group D1, D2, E2.1 and E2.2 against SARS-CoV-2 D614G and Omicron subvariants (BA.1, BA.1.1, BA.3, BA.2, BA.2.13, BA.2.12.1, BA.4/BA.5) spike-pseudotyped VSV. Geometric mean of IC50 (μg/mL) are annotated above the bars. P-values were calculated using a two-tailed Wilcoxon singed-rank test, in comparison to IC50 against BA.2. c, Neutralizing activity of antibodies in group D1, D2, E2.1 and E2.2 against SARS-CoV-2 D614G, in addition to D614G+L452M, D614G+L452Q and D614G+L452R. Geometric mean of IC50 fold changes compared to IC50 against D614G are annotated above the bars. P-values were calculated using a two-tailed Wilcoxon signed-rank test. *, <0.05; **, <0.01; ***, <0.001; n.s., not significant. d, Averaged escape maps at escape hotspots of antibodies in epitope group D1, D2, E2.1 and E2.2, and corresponding MSA of various sarbecovirus RBDs. Height of each amino acid in the escape maps represents its mutation escape score. Mutated sites in Omicron variants are marked in bold.

Figure 5

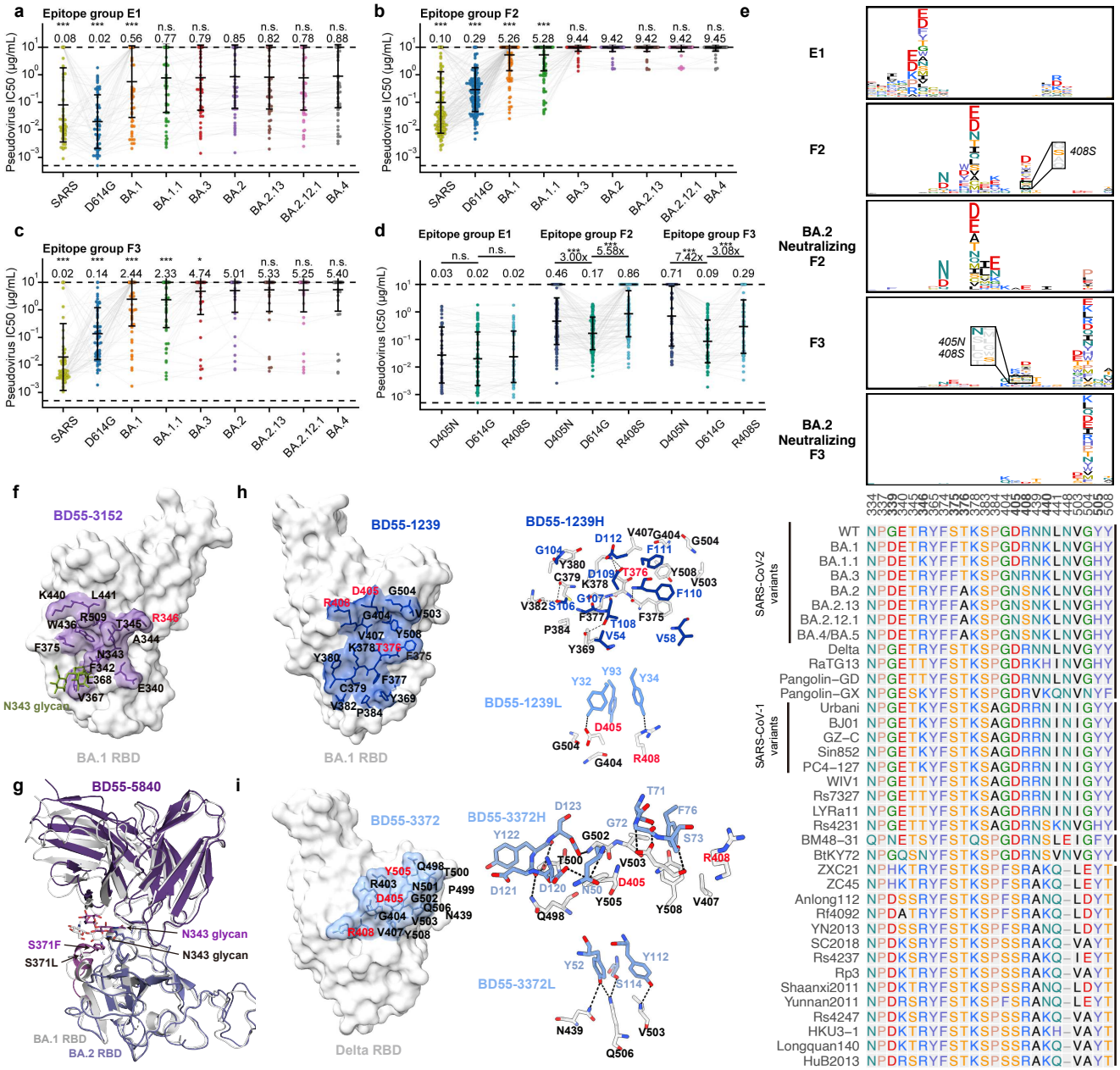

Fig. 5 | BA.2 subvariants escape broad sarbecovirus neutralizing antibodies

a-c, Neutralizing activity against SARS-CoV-1, SARS-CoV-2 D614G and Omicron subvariants by antibodies in group E1 (a), F2 (b) and F3 (c). Geometric mean of IC50 (μg/mL) are annotated above the bars. P-values were calculated using a two-tailed Wilcoxon signed-rank test, in comparison to IC50 against BA.2. d, Neutralizing activity of antibodies in group E1, F2 and F3 against SARS-CoV-2 D614G, in addition to D614G+D405N and D614G+R408S. Geometric mean of IC50 fold changes compared to IC50 against D614G are annotated above the bars. P-values were calculated using a two-tailed Wilcoxon signed-rank test. *, <0.05; **, <0.01; ***, <0.001; n.s., not significant. e, Average escape maps of group E1 antibodies, in addition to all antibodies and BA.2-neutralizing antibodies (BA.2 IC50 < 2μg/mL) in epitope group F2 and F3, and corresponding multiple sequence alignment (MSA) of various sarbecovirus RBDs. Height of each amino acid in the escape maps represents its mutation escape score. Mutated sites in Omicron subvariants are marked in bold. f, Epitope of Group E1 antibody BD55-3152 on SARS-CoV-2 BA.1 RBD. g, Structural overlay of the BD55-5840 in complex of BA.1 and BA.2 RBD. The 366-377 hairpin and N343 glycan in BA.2 RBD are highlighted. h-i, Epitope and interactions on the binding interface of BD55-1239 (Group F2) and BD55-3372 (Group F3), in complex of BA.1 RBD. Residues of the antibody are blue, and RBD residues are black or red. Residues highlighted in red indicate mutated sites in Omicron variants.

Figure 6

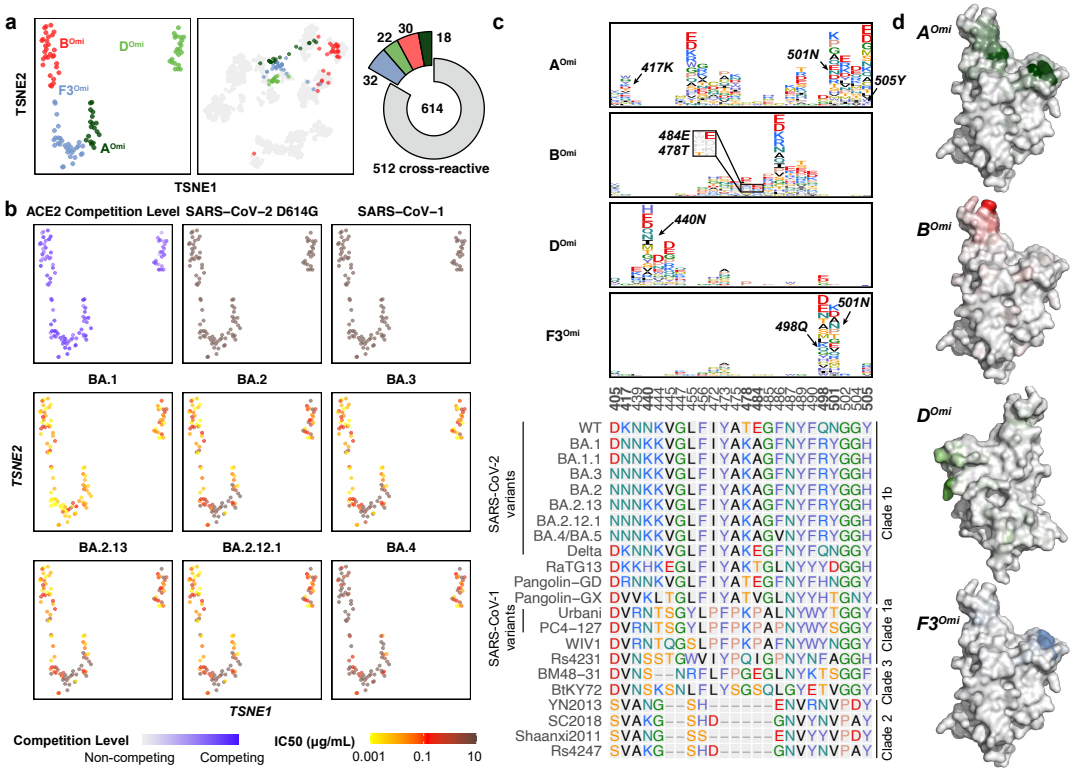

Fig. 6 | BA.1-specific antibodies elicited by BA.1 infection are evaded by Omicron subvariants

a, Four epitope groups were identified from DMS profiles of 102 neutralizing antibodies that do not bind to wildtype RBD from BA.1 convalescents. b, Functional mapping of the 102 BA.1-specific antibodies, including ACE2 competition and neutralizing activity against SARS-CoV-1, SARS-CoV-2 D614G, and Omicron subvariants. c, Averaged escape maps at escape hotspots of the 102 antibodies in four epitope groups, and corresponding MSA of various sarbecovirus RBDs. Height of each amino acid in the escape maps represents its mutation escape score. Mutated sites in Omicron variants are marked in bold. Detected wildtype-related escaping mutations are highlighted. d, Average escape scores of each BA.1-specific epitope group and each residue on the RBD are projected onto the structure of BA.1 RBD (PDB: 7WPB).

Extended Data Fig. 1

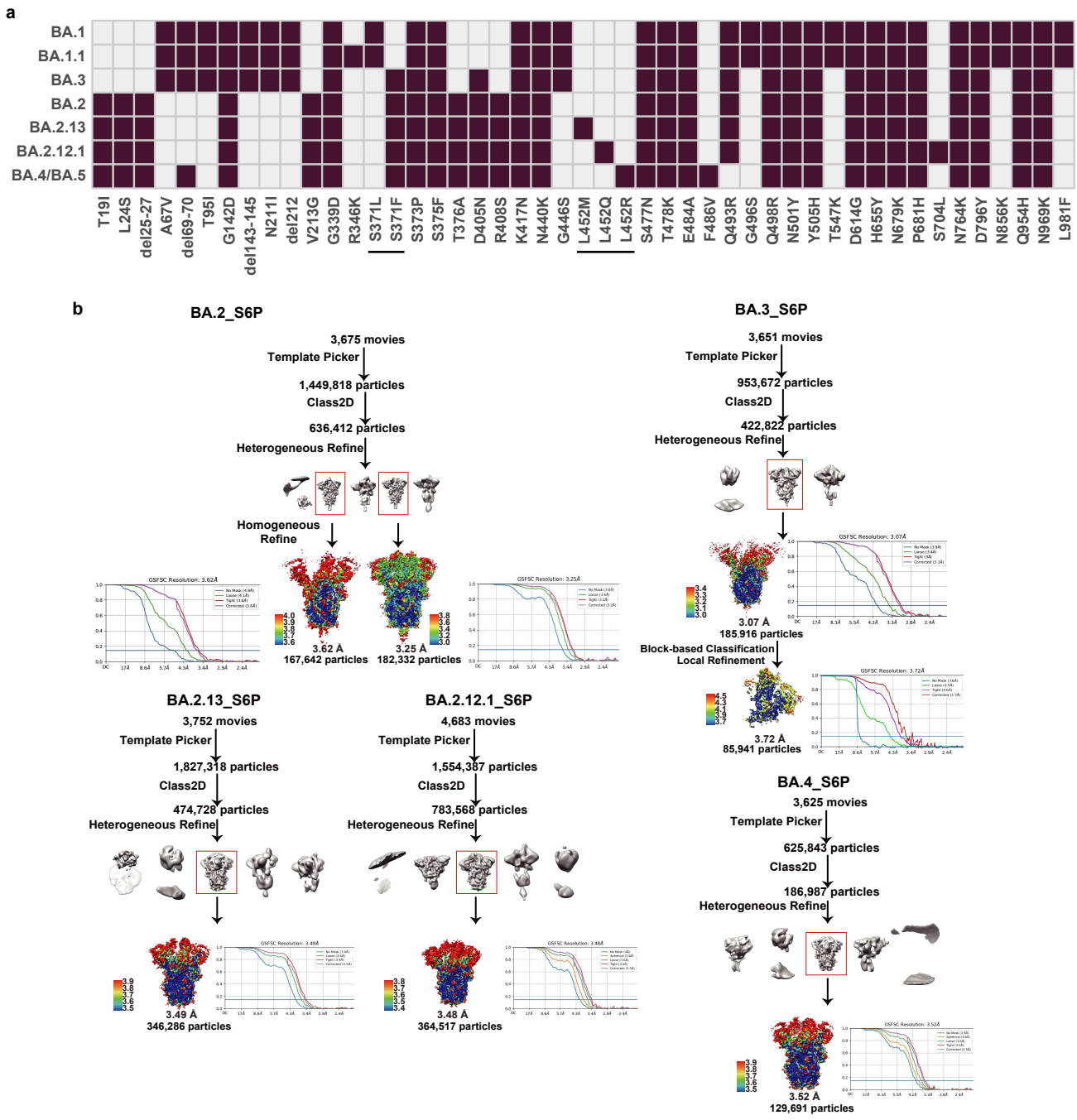

Extended Data Fig. 1 | Spike mutations of emerging Omicron subvariants.
a, Mutations on the spike glycoprotein of SARS-CoV-2 Omicron subvariants. b, Workflow to generate cryo-EM structure of BA.2, BA.3, BA.2.13, BA.2.12.1, BA.4 spike glycoprotein trimer with S6P and R683A, R685A substitutions.

Extended Data Fig. 2

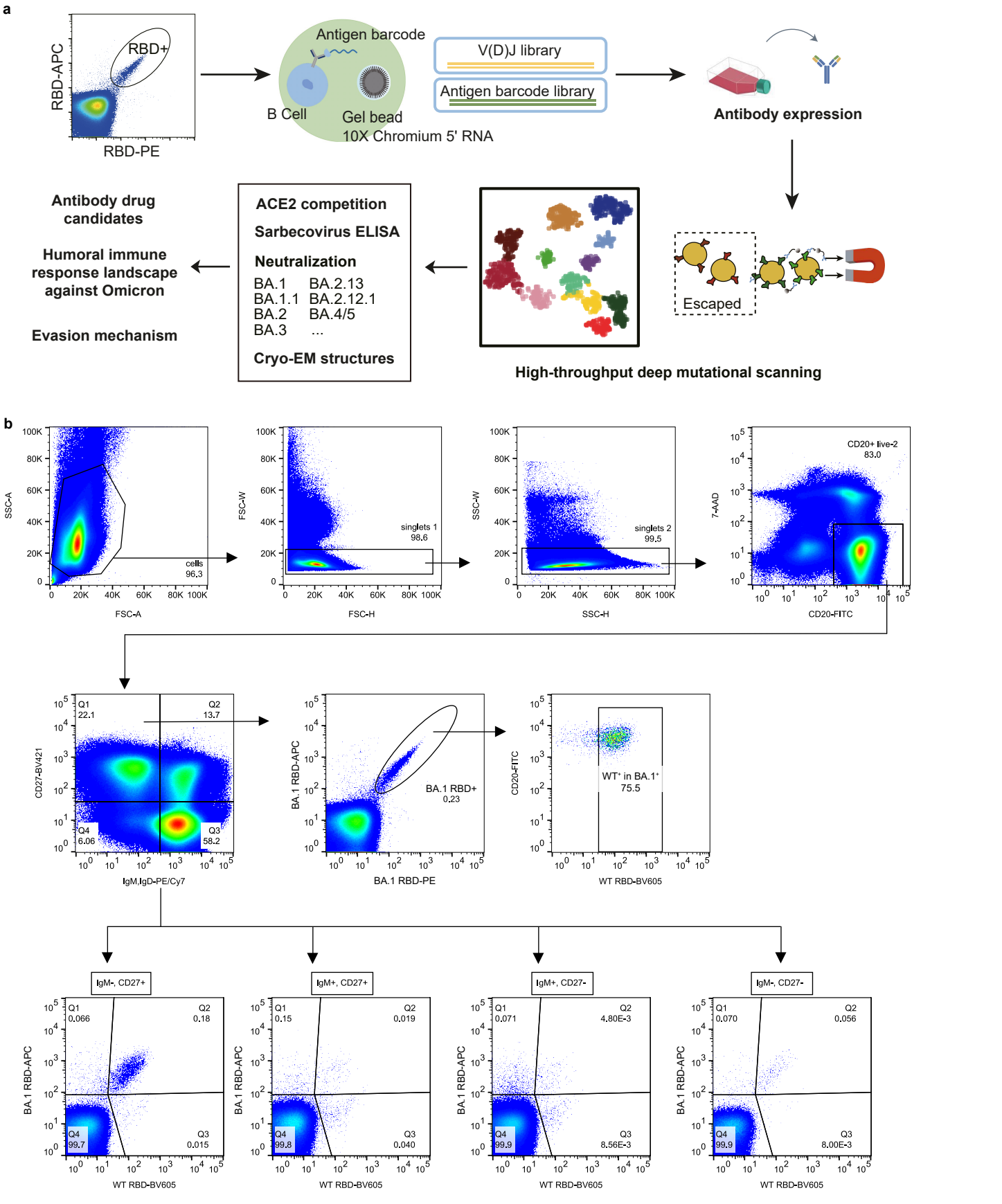

Extended Data Fig. 2 | Workflow for the isolation and characterization of SARS-CoV-2 RBD antibodies. a, Overall pipeline of antibody identification by single cell VDJ sequencing with feature barcodes and epitope analysis by high-throughput deep mutational scanning. b, FACS strategy to enrich BA.1/WT bivalent memory B cells or BA.1-specific memory B cells.

Extended Data Fig. 3

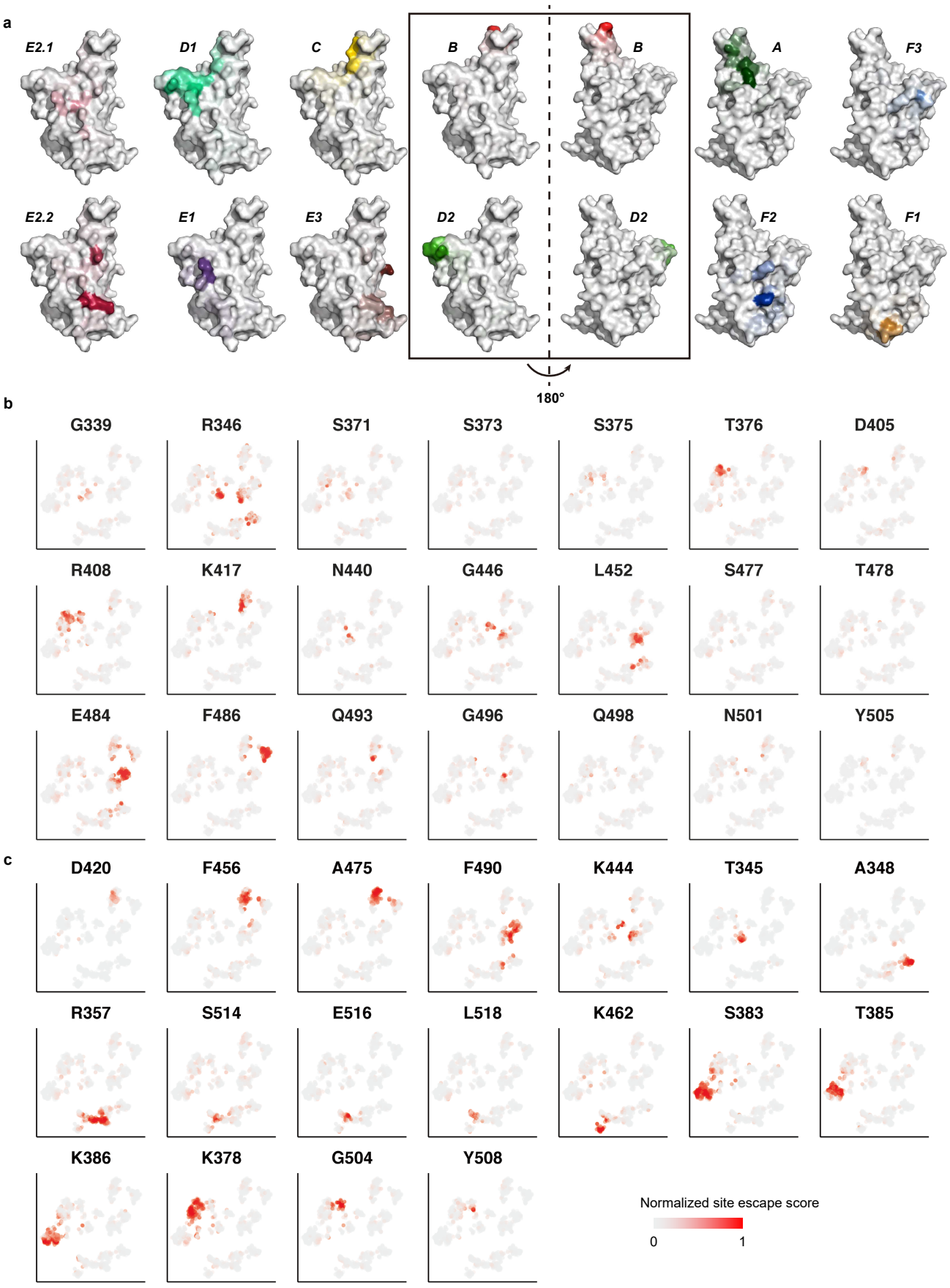

Extended Data Fig. 3 | Escape hotspots of various epitope groups.

a, Average escape scores of each epitope group and each residue on the RBD are projected onto the structure of SARS-CoV-2 RBD. b-c, Site total escape scores of mutated residues in Omicron variants (b) and feature residues of each group (c) are projected onto the t-SNE. Shades of red indicate normalized site total escape scores of the representative residues for each antibody.

Extended Data Fig. 4

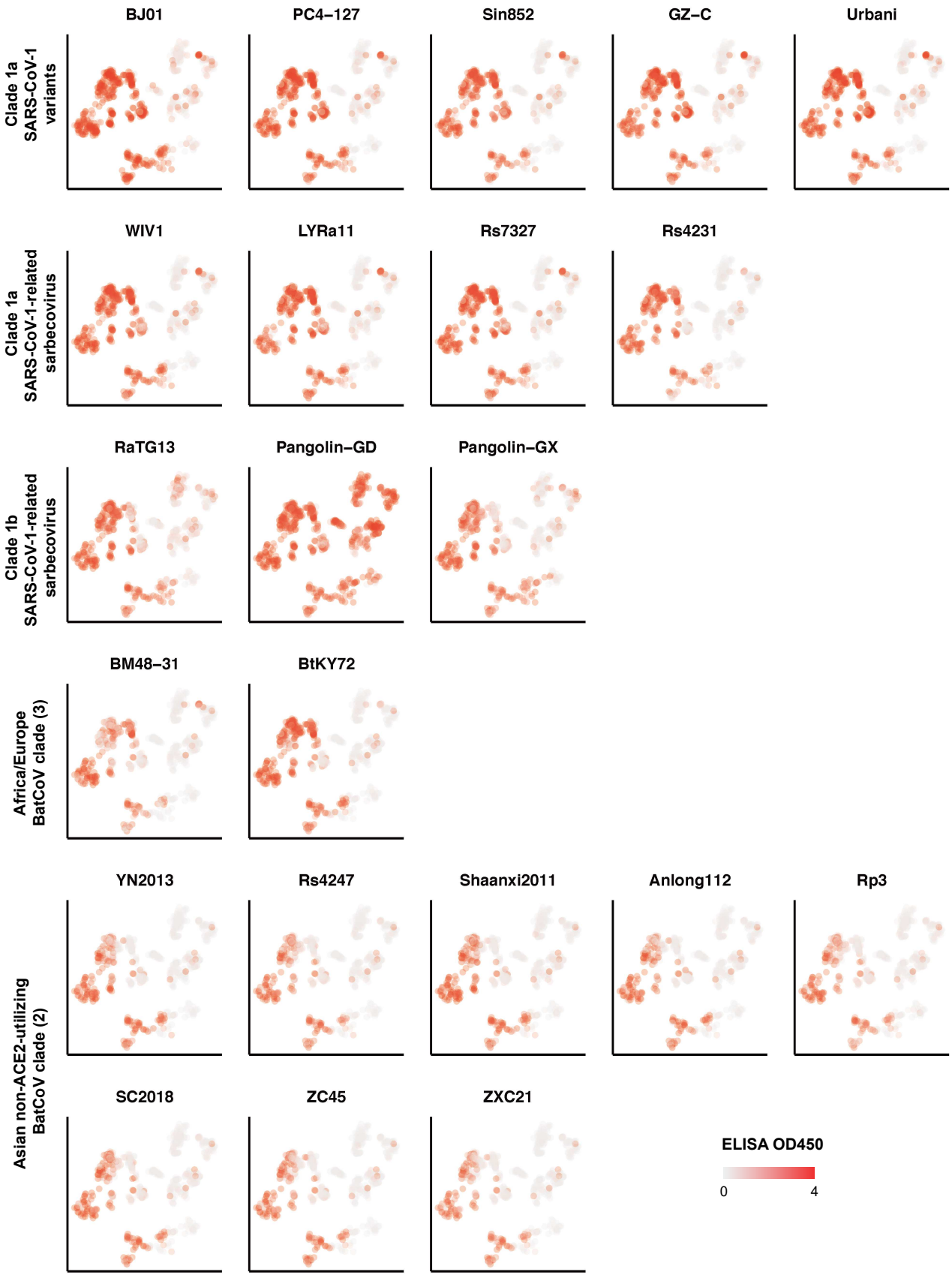

Extended Data Fig. 4 | ELISA reactivity against 22 sarbecovirus RBD.
Shades of red indicate ELISA OD450 for each antibody against various sarbecovirus from different clades.

Extended Data Fig. 5

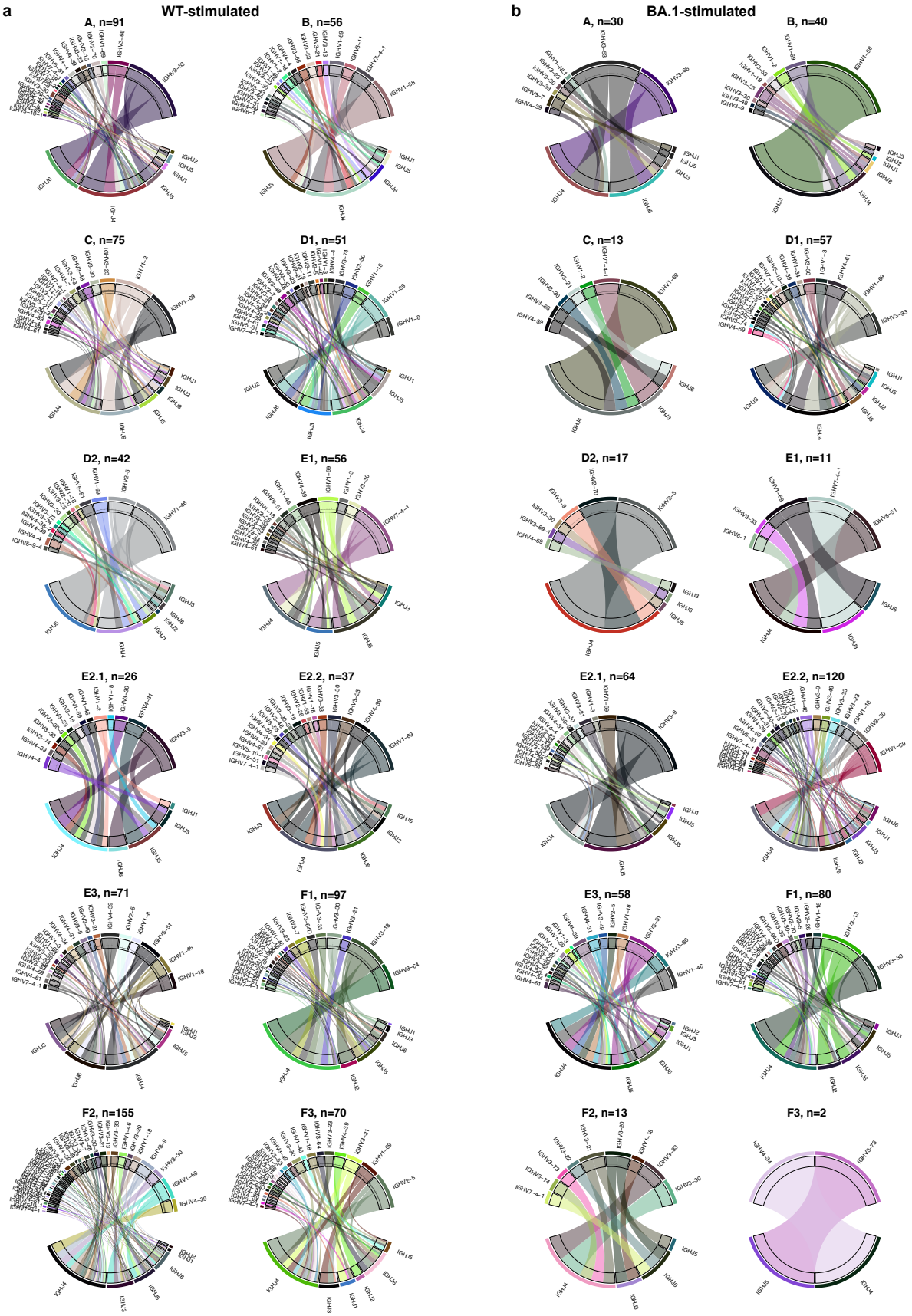

Extended Data Fig. 5 | Heavy chain V-J genes of BA.1-stimulated and WT-stimulated antibodies in each epitope group.

Heavy chain V-J genes combination of a, WT-stimulated antibodies. b, BA.1-stimulated antibodies. Number of antibodies in each group is annotated above the chord plot.

Extended Data Fig. 6

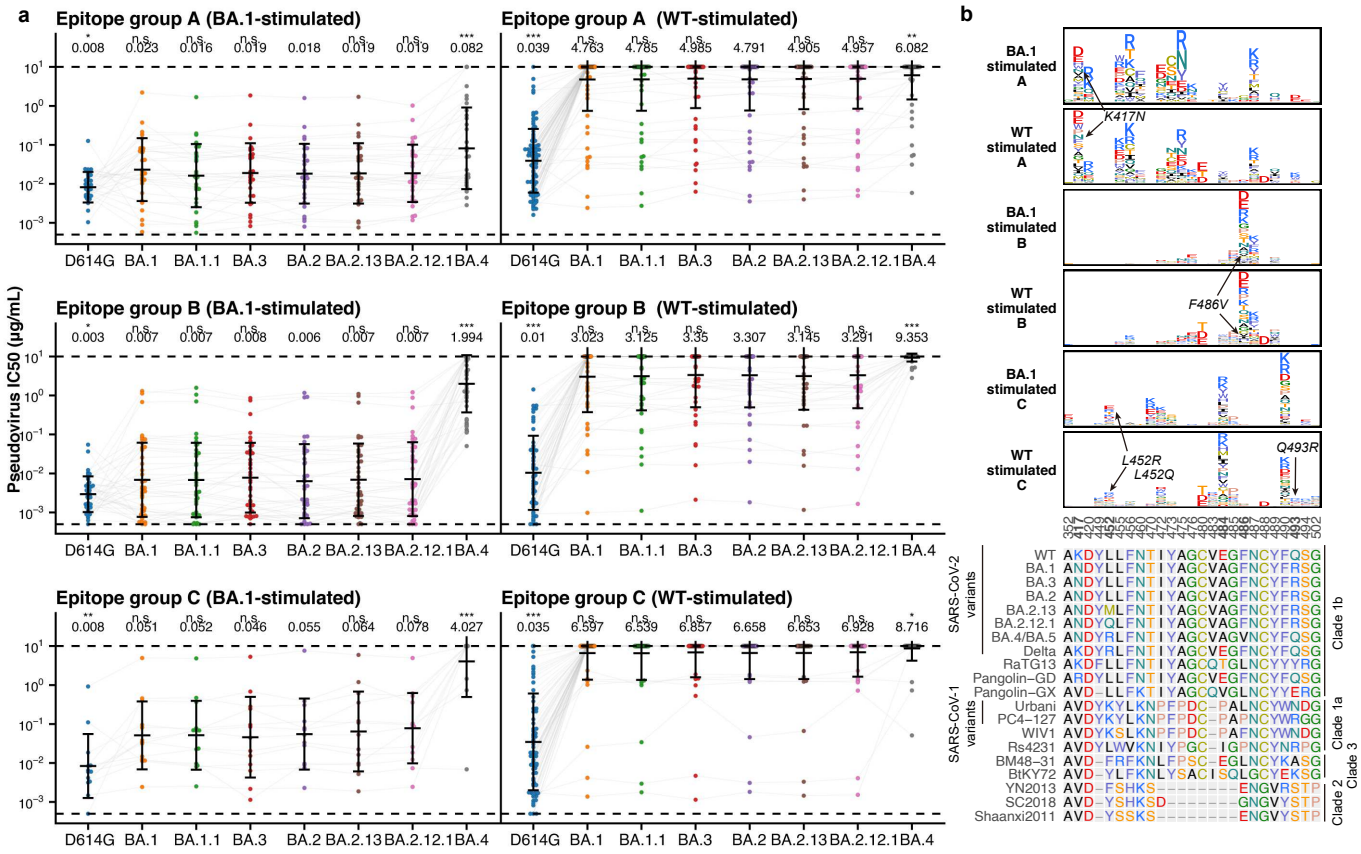

Extended Data Fig. 6 | Comparison of BA.1-stimulated and WT-stimulated antibodies in group A, B and C.

a, Neutralizing activity against SARS-CoV-2 D614G and Omicron subvariants by BA.1-stimulated and WT-stimulated antibodies in group A, B and C. Geometric mean of IC50 (μg/mL) are annotated above the bars. P-values were calculated using a two-tailed Wilcoxon signed-rank test, in comparison to IC50 against BA.2. b, Averaged escape maps at escape hotspots of BA.1-stimulated and WT-stimulated antibodies in group A, B and C, and corresponding MSA of various sarbecovirus RBDs. Height of each amino acid in the escape maps represents its mutation escape score. Mutated sites in Omicron variants are marked in bold.

Extended Data Fig. 7

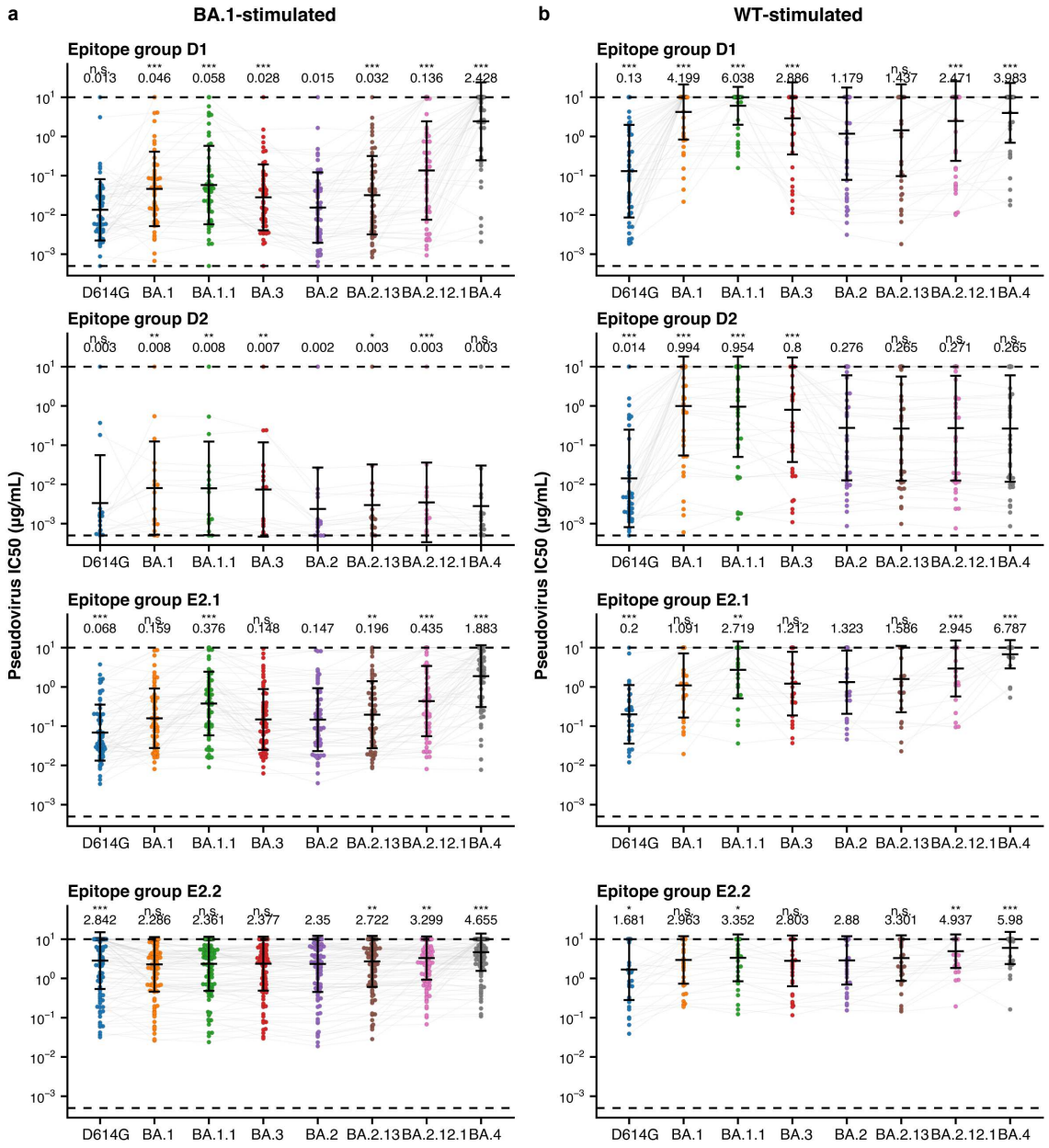

Extended Data Fig. 7 | Neutralization by BA.1-stimulated and WT-stimulated antibodies in group D1, D2, E2.1 and E2.2.

a-b, Neutralizing activity against SARS-CoV-2 D614G and Omicron subvariants by BA.1-stimulated (a) and WT-stimulated antibodies (b) in group D1, D2, E2.1 and E2.2. Geometric mean of IC50 (μg/mL) are annotated above the bars. P-values were calculated using a two-tailed Wilcoxon signed-rank test, in comparison to IC50 against BA.2.

Extended Data Fig. 8

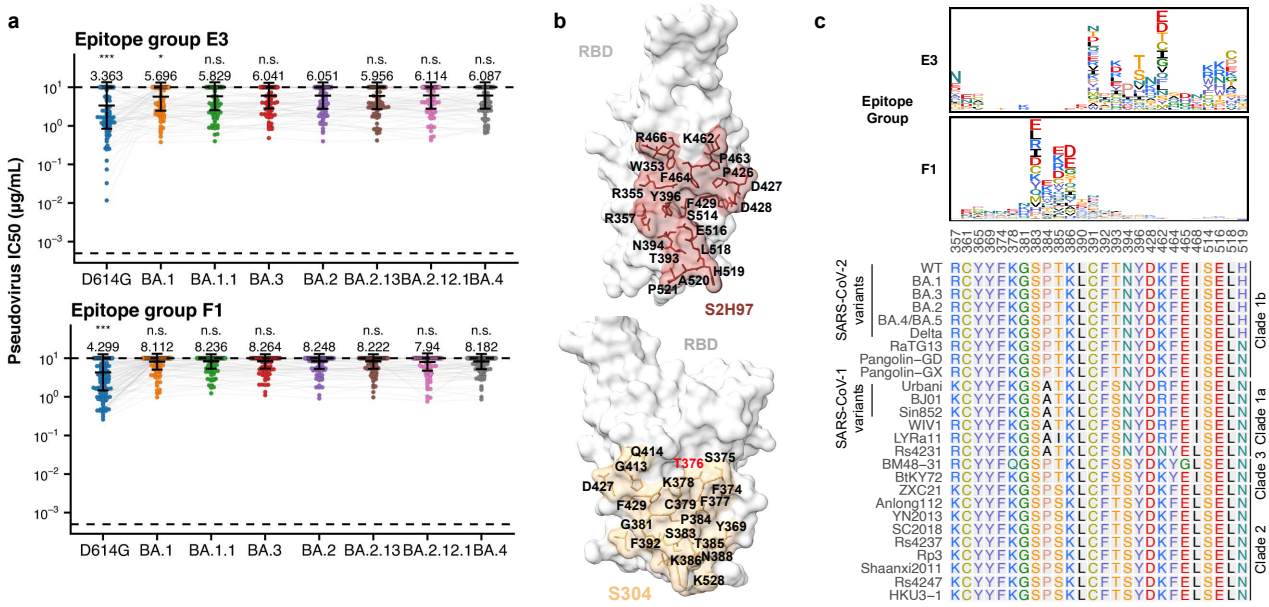

Extended Data Fig. 8 | Antibodies of group E3 and F1 exhibit weak but broad-spectrum neutralization. a, Neutralizing activity against SARS-CoV-2 D614G and Omicron subvariants by antibodies in group E3 and F1. Geometric mean of IC50 (μg/mL) are annotated above the bars. P-values were calculated using a two-tailed Wilcoxon signed-rank test, in comparison to IC50 against BA.2. b, Epitope of representative antibodies in group E3 (S2H97, PDB: 7M7W) and F1 (S304, PDB: 7JW0). Residues highlighted in red indicate mutated sites in Omicron variants. c, Averaged escape maps at escape hotspots of antibodies in group E3 and F1, and corresponding MSA of various sarbecovirus RBDs. Height of each amino acid in the escape maps represents its mutation escape score. Mutated sites in Omicron variants are marked in bold.

Extended Data Fig. 9

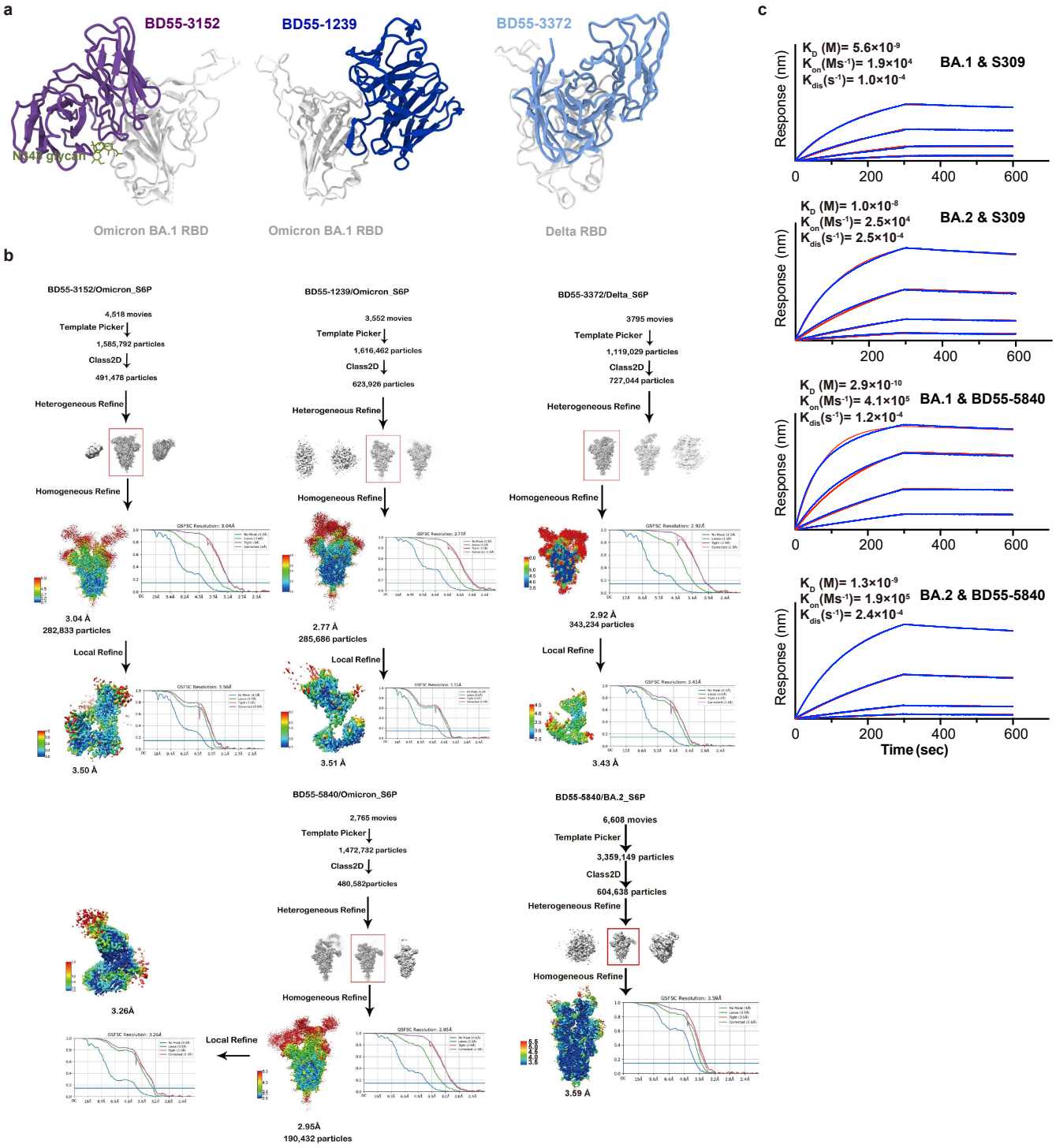

Extended Data Fig. 9 | RBD-binding structures and affinity of broad Sarbecovirus antibodies.
a, Cartoon models of Cryo-EM structures of BD55-3152 in complex of BA.1 RBD, BD55-1239 in complex of BA.1 RBD, and BD55-3372 in complex of Delta RBD. b, Workflow to generate refined structural model of BD55-3152 and BD55-1239 in complex of BA.1 RBD, BD55-3372 in complex of Delta RBD, and BD55-5840 in complex of BA.2 RBD. c, Biolayer interferometry analysis of Group E1 antibodies S309 and BD55-5840 binding to Omicron BA.1 and BA.2 Spike trimer.

Extended Data Fig. 10

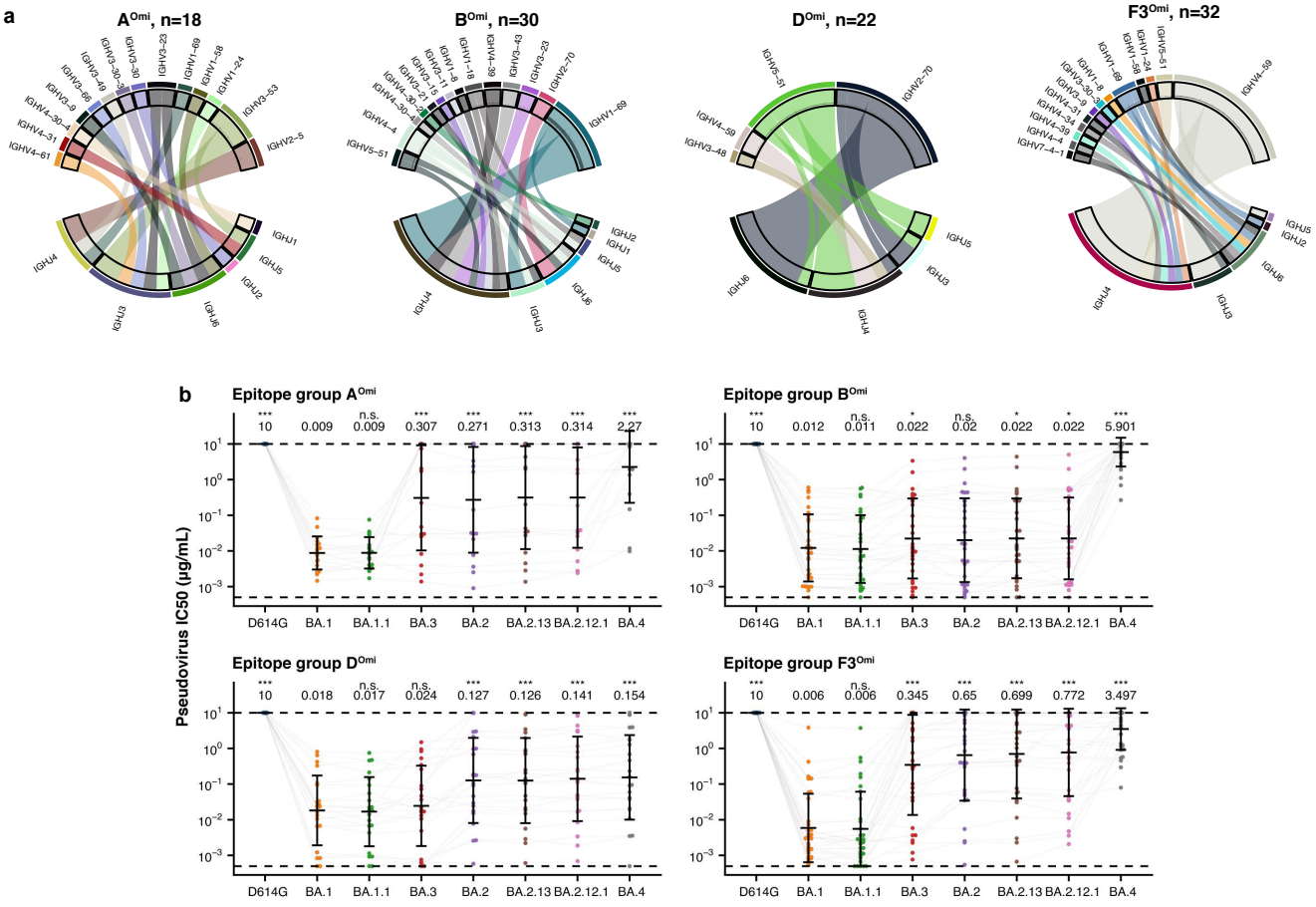

Extended Data Fig. 10 | HV-HJ gene combination and neutralizing activities of BA.1-specific antibodies. a, Heavy chain V-J gene combination of BA.1-specific neutralizing antibodies in BA.1-specific epitope groups A^{Omi}, B^{Omi}, D^{Omi} and $F3^{Omi}$. b, Neutralizing activity against SARS-CoV-2 D614G and Omicron subvariants by BA.1-specific neutralizing antibodies in BA.1-sepcific epitope groups. Geometric mean of IC50 (μg/mL) are annotated above the bars. P-values were calculated using a two-tailed Wilcoxon signed-rank test, in comparison to IC50 against BA.1.

Methods

Plasma and PBMC isolation

Blood samples were obtained from 40 volunteers who received 3 doses of CoronaVac, 39 individuals who received 2 doses of CoronaVac and 1 booster dose of ZF2001, 54 BA.1 convalescents who had received 3 doses of CoronaVac before BA.1 infection[39,40], and 30 SARS convalescents who received 2 doses of CoronaVac and 1 dose of ZF2001. The volunteers' blood samples were obtained 4 weeks after the booster shot or 4 weeks after discharge from the hospital after BA.1 infection. Relevant experiments regarding SARS convalescents and SARS-CoV-2 vaccinees were approved by the Beijing Ditan Hospital Capital Medical University (Ethics committee archiving No. LL-2021-024-02), the Tianjin Municipal Health Commission, and the Ethics Committee of Tianjin First Central Hospital (Ethics committee archiving No. 2022N045KY). Written informed consent was obtained from each participant in accordance with the Declaration of Helsinki. All participants provided written informed consent for the collection of information, storage and usage of their clinical samples for research purpose, and publication of data generated from this study.

Whole blood samples were mixed and subjected to Ficoll (Cytiva, 17-1440-03) gradient centrifugation after 1:1 dilution in PBS+2% FBS to isolate plasma and peripheral blood mononuclear cells (PBMC). After centrifugation, plasma was collected from upper layer and cells were harvested at the interface, respectively. PBMCs were further prepared through centrifugation, red blood cells lysis (InvitrogenTM eBioscienceTM 1X RBC Lysis Buffer, 00-4333-57) and washing steps. Samples were stored in FBS (Gibco) with 10% DMSO (Sigma) in liquid nitrogen if not used for downstream process immediately. Cryopreserved PBMCs were thawed in DPBS+2% FBS (Stemcell, 07905).

Antibody isolation and recombinant production

SARS-CoV-1 and SARS-CoV-2 RBD cross-binding memory B cells were isolated from PBMC of SARS-CoV-1 convalescents who received SARS-CoV-2 vaccine and BA.1 infected

convalescents who had been vaccinated against COVID-19 prior to infection. Briefly, CD19+ B cells were isolated from PBMC with EasySep™ Human CD19 Positive Selection Kit II (STEMCELL, 17854). B cells were then stained with FITC anti-human CD19 antibody (BioLegend, 392508), FITC anti-human CD20 antibody (BioLegend, 302304), Brilliant Violet 421™ anti-human CD27 antibody (BioLegend, 302824), PE/Cyanine7 anti-human IgM antibody (BioLegend, 314532), biotinylated Ovalbumin (SinoBiological) conjugated with Brilliant Violet 605™ Streptavidin (BioLegend, 405229), SARS-CoV-1 biotinylated RBD protein (His & AVI Tag) (SinoBiological, 40634-V27H-B) conjugated with PE-streptavidin (BioLegend, 405204), SARS-CoV-2 biotinylated RBD protein (His & AVI Tag) (SinoBiological, 40592-V27H-B) conjugated with APC-streptavidin (BioLegend, 405207), and 7-AAD (Invitrogen, 00-6993-50). 7-AAD-, CD19/CD20+, CD27+, IgM-, OVA-, SARS-COV-1 RBD+, and SARS-CoV-2 RBD+ were sorted with MoFlo Astrios EQ Cell Sorter (Beckman Coulter).

SARS-CoV-2 BA.1 RBD binding memory B cells were isolated from BA.1 infected convalescents who received SARS-CoV-2. Briefly, CD19+ B cells were isolated with EasySep™ Human CD19 Positive Selection Kit II. B cells were then stained with FITC anti-human CD20 antibody, Brilliant Violet 421™ anti-human CD27 antibody, PE/Cyanine7 anti-human IgM antibody, PE/Cyanine7 anti-human IgD antibody(BioLegend, 348210), biotinylated SARS-CoV-2 BA.1 protein (His & AVI Tag) (SinoBiological, 40592-V49H7-B) conjugated with PE-streptavidin, APC-streptavidin, TotalSeq™-C0971 Streptavidin (BioLegend, 405271), and TotalSeq™-C0972 Streptavidin (BioLegend, 405273), SARS-CoV-2 biotinylated RBD protein (His & AVI Tag) conjugated with Brilliant Violet 605™ Streptavidin, TotalSeq™-C0973 Streptavidin(BioLegend, 405275), TotalSeq™-C0974 Streptavidin(BioLegend, 405277), biotinylated Ovalbumin conjugated with TotalSeq™-C0975 Streptavidin(BioLegend, 405279) and 7-AAD. 7-AAD-, CD20+, CD27+, IgM-, IgD-, SARS-CoV-2 BA.1 RBD+ were sorted with MoFlo Astrios EQ Cell Sorter. FACS data were analyzed using FlowJo™ v10.8 (BD Biosciences).

Sorted B cells were then processed with Chromium Next GEM Single Cell V(D)J Reagent Kits v1.1 following the manufacturer's user guide (10x Genomics, CG000208). Briefly, Cells sorted

were resuspended in PBS after centrifugation. Gel beads-in-emulsion (GEMs) were obtained with 10X Chromium controller and then subjected to reverse transcription (RT). After GEM-RT clean up, RT products were subject to preamplification. After amplification and purification with SPRIselect Reagent Kit (Beckman Coulter, B23318) of RT products, B cell receptor (BCR) sequence (paired V(D)J) were enriched with 10X BCR primers. After library preparation, libraries were sequenced by Novaseq 6000 platform running Novaseq 6000 S4 Reagent Kit v1.5 300 cycles (Illumina, 20028312) or NovaSeq XP 4-Lane Kit v1.5 (Illumina, 20043131).

B cell RNA and feature barcode data analysis

Using Cell Ranger (v6.1.1) pipeline, the mRNA fastq reads were processed and aligned to the human GRCh38 genome for gene expression profile. Genes expressed in less than 10 cells and cells expressed less than 100 genes or high-level mitochondria genes were removed, to filter out low-quality data. Raw counts were normalized and scaled with Seurat[41] (v 4.0.3), while principal components analysis (PCA) and uniform manifold approximation and projection (UMAP) were performed for cluster and visualization. Cell types were identified using SingleR[42] (v1.6.1) with Monaco human immune reference[43]. Feature barcode reads were also counted by Cell Ranger (v6.1.1) as antibody capture library, and a cell was considered to bind the corresponding antigen of dominant feature barcodes (>25% in this cell).

Antibody sequence analysis

The antibody sequences obtained from 10X Genomics V(D)J sequencing were aligned to GRCh38 reference and assembled as immunoglobulin contigs by the Cell Ranger (v6.1.1) pipeline. Non-productive contigs and B cells that had multiple heavy chain or light chain contigs were filtered out of the analysis. V(D)J gene annotation was performed using NCBI IgBlast (v1.17.1) with the IMGT reference. Mutations on V(D)J nucleotide sequences were calculated by using the igpipeline, which compared the sequences to the closest germline genes and counted the number of different nucleotides. For antibodies from public sources whose original sequencing nucleotide sequences were not all accessible, the antibody amino acid sequences were annotated by

IMGT/DomainGapAlign[44] (v4.10.2) with default parameters. The V-J pairs were visualized by R package circlize (v0.4.10).

Deep Mutational Scanning Library construction

Deep mutational scanning libraries were constructed as previously described[3]. Briefly, SARS-CoV-2 RBD mutant libraries were constructed from Wuhan-Hu-1 RBD sequence (GenBank: MN908947, residues N331-T531), and Omicron RBD mutant libraries were created in a similar way based on Wuhan-Hu-1 RBD sequence with the addition of G339D, S371L, S373P, S375F, K417N, N440K, G446S, S477N, T478K, E484A, Q493R, G496S, Q498R, N501Y, and Y505H mutations. Duplicated libraries were independently produced, theoretically containing 3819 possible amino acid mutations. Each RBD mutant was barcoded with a unique 26-nucleotide (N26) sequence and Pacbio sequencing was used to identify the correspondence of RBD mutant and N26 barcode. After mutant library transformation, ACE2 binders were enriched for downstream mutation profile experiment.

High-throughput antibody-escape mutation profiling

The previously described high-throughput MACS (magnetic-activated cell sorting)-based antibody-escape mutation profiling system[3,17] was used to characterize mutation escape profile for neutralizing antibodies. Briefly, ACE2 binding mutants were induced overnight for RBD expression and washed followed by two rounds of Protein A antibody based negative selection and MYC-tag based positive selection to enrich RBD expressing cells. Protein A antibody conjugated products were prepared following the protocol of Dynabeads Protein A (Thermo Fisher, 10008D) and incubated with induced yeast libraries at room temperature for 30min with shaking. MYC-tag based positive selection was performed according to the manufacturer's instructions (Thermo Fisher, 88843).

After three rounds of sequential cell sorting, the obtained cells were recovered overnight. Plasmids were extracted from pre- and post-sort yeast populations by 96-Well Plate Yeast Plasmid Preps

Kit (Coolaber, PE053). The extracted plasmids were then used to amplify N26 barcode sequences by PCR. The final PCR products were purified with 1X AMPure XP magnetic beads (Beckman Coulter, A63882) and submitted to 75bp single-end sequencing at Illumina Nextseq 500 platform.

Processing of deep mutational scanning data

Single-end Illumina sequencing reads were processed as previously described. Briefly, reads were trimmed into 16 or 26 bp and aligned to the reference barcode-variant dictionary with dms_variants package (v0.8.9). Escape scores of variants were calculated as $F\times(n_{X,ab} / N_{ab}) / (n_{X,ref} / N_{ref})$, where $n_{X,ab}$ and $n_{X,ref}$ is the number of reads representing variant X, and N_{ab} and N_{ref} are the total number of valid reads in antibody-selected (ab) and reference (ref) library, respectively. F is a scale factor defined as the 99th percentiles of escape fraction ratios. Variants detected by less than 6 reads in the reference library were removed to avoid sampling noise. Variants containing mutations with ACE2 binding below -2.35 or RBD expression below -1 were removed as well, according to data previously reported. For $RBD^{BA.1}$-based libraries, due to the lack of corresponding ACE2 binding and RBD expression data, we used the RBD expression of RBD^{Beta}-based DMS as filter instead[45], and did not perform the ACE2-binding filter. Mutations on residues that use different amino acids in Beta and BA.1 are not filtered, except R493P, S496P, R498P, H505P and all mutations on F375, which were excluded in the analysis due to low expression. Finally, global epistasis models were built using dms_variants package to estimate mutation escape scores. For most antibodies, at least two independent assays are conducted and single mutation escape scores are averaged across all experiments that pass quality control.

Antibody clustering and visualization

Site total escape scores, defined as the sum of escape scores of all mutations at a particular site on RBD, were used to evaluate the impact of mutations on each site for each antibody. Each of these scores is considered as a feature of a certain antibody and used to construct a feature matrix $\mathbf{A}_{N\times M}$ for downstream analysis, where N is the number of antibodies and M is the number of features (valid sites). Informative sites were selected using sklearn.feature_selection.VarianceThreshold of

scikit-learn Python package (v0.24.2) with the variance threshold as 0.1. Then, the selected features were L2-normalized across antibodies using sklearn.preprocessing.normalize. The resulting matrix is referred as $\mathbf{A'}_{N\times M'}$, where M' is the number of selected features. The dissimilarity of two antibodies i, j is defined as 1-Corr($\mathbf{A'}_i$,$\mathbf{A'}_j$), where Corr(**x**,**y**) is the Pearson's correlation coefficient of vector **x** and **y**. We used sklearn.manifold.MDS to reduce the number of features from M' to D=20 with multidimensional scaling under the above metric. Antibodies are clustered into 12 epitope groups using sklearn.cluster.KMeans of scikit-learn in the resulting D-dimensional feature space. Finally, these D-dimensional representations of antibodies were further embedded into two-dimensional space for visualization with t-SNE using sklearn.manifold.TSNE of scikit-learn. For the 102 BA.1-specific antibodies that were assayed with $RBD^{BA.1}$-based yeast display library, the 20-dimensional embedding were generated using MDS with all 1640 antibodies' DMS profile, but clustering and t-SNE were conducted independently. To project these antibodies onto the t-SNE space of 1538 antibodies assayed by RBD^{WT}-based DMS, we calculated the pairwise Euclidean distance between 102 antibodies using $RBD^{BA.1}$-based DMS and 1538 antibodies using RBD^{WT}-based DMS in the 20-dimensional MDS space. The position of each BA.1-specific antibody in the original t-SNE space is defined as the average position of its ten nearest antibodies using RBD^{WT}-based DMS. All t-SNE plots were generated by R package ggplot2 (v3.3.3).

Pseudovirus neutralization assay

SARS-CoV-2 spike (GenBank: MN908947), Pangolin-GD spike (GISAID: EPI_ISL_410721), RaTG13 spike (GISAID: EPI_ISL_402131), SARS-CoV-1 spike (GenBank: AY278491), Omicron BA.1 spike (A67V, H69del, V70del, T95I, G142D, V143del, Y144del, Y145del, N211del, L212I, ins214EPE, G339D, S371L, S373P, S375F, K417N, N440K, G446S, S477N, T478K, E484A, Q493R, G496S, Q498R, N501Y, Y505H, T547K, D614G, H655Y, N679K, P681H, N764K, D796Y, N856K, Q954H, N969K, L981F), BA.2 spike (GISAID: EPI_ISL_7580387, T19I, L24S, del25-27, G142D, V213G, G339D, S371F, S373P, S375F,

T376A, D405N, R408S, K417N, N440K, G446S, S477N, T478K, E484A, Q493R, Q498R, N501Y, Y505H, D614G, H655Y, N679K, P681H, N764K, D796Y, Q954H, N969K), BA.1.1 spike (BA.1+R346K), BA.3 spike (A67V, del69-70, T95I, G142D, V143del, Y144del, Y145del, N211del, L212I, G339D, S371F, S373P, S375F, D405N, K417N, N440K, G446S, S477N, T478K, E484A, Q493R, Q498R, N501Y, Y505H, D614G, H655Y, N679K, P681H, N764K, D796Y, Q954H, N969K), BA.2.12.1 spike (BA.2+L452Q+S704L), BA.2.13 spike (BA.2+L452M), BA.4 spike (T19I, L24S, del25-27, del69-70, G142D, V213G, G339D, S371F, S373P, S375F, T376A, D405N, R408S, K417N, N440K, G446S, L452R, S477N, T478K, E484A, F486V, Q498R, N501Y, Y505H, D614G, H655Y, N679K, P681H, N764K, D796Y, Q954H, N969K) plasmid is constructed into pcDNA3.1 vector. G*ΔG-VSV virus (VSV G pseudotyped virus, Kerafast) is used to infect 293T cells (American Type Culture Collection [ATCC], CRL-3216), and spike protein expressing plasmid was used for transfection at the same time. After culture, the supernatant containing pseudovirus was harvested, filtered, aliquoted, and frozen at −80°C for further use.

Pseudovirus detection of Pangolin-GD and RaTG13 was performed in 293T cells overexpressing human angiotensin-converting enzyme 2 (293T-hACE2 cells). Other pseudovirus neutralization assays were performed using the Huh-7 cell line (Japanese Collection of Research Bioresources [JCRB], 0403).

Monoclonal antibodies or plasma were serially diluted (5-fold or 3-fold) in DMEM (Hyclone, SH30243.01) and mixed with pseudovirus in 96-well plates. After incubation at 5% CO_2 and 37°C for 1 h, digested Huh-7 cell (Japanese Collection of Research Bioresources [JCRB], 0403) or 293T-hACE2 cells (AmericanTypeCultureCollection[ATCC],CRL-3216) were seeded. After 24 hours of culture, supernatant was discarded and D-luciferin reagent (PerkinElmer, 6066769) was added to react in the dark, and the luminescence value was detected using a microplate spectrophotometer (PerkinElmer, HH3400). IC50 was determined by a four-parameter logistic regression model.

ELISA

To detect the broad-spectrum binding of the antibodies among Sarbecovirus, we entrusted SinoBiological Technology Co., Ltd. to synthesize a panel of 20 sarbecovirus RBDs (Supplementary Table 3). According to the sequence of 20 RBDs, a set of nested primers was designed. The coding sequences were obtained by the overlap-PCR with a 6xHis tag sequence to facilitate protein purification. The purified PCR products were ligated to the secretory expression vector pCMV3 with CMV promoter, and then transformed into E. coli competent cells XL1-blue. Monoclones with correct transformation were cultured and expanded, and plasmids were extracted. Healthy HEK293 cells were passaged into a new cell culture and grown in suspension at 37 °C, 120 RPM, 8% CO2 to logarithmic growth phase and transfected with the recombinant constructs by using liposomal vesicles as DNA carrier. After transfection, the cell cultures were followed to assess the kinetics of cell growth and viability for 7 days. The cell expression supernatant was collected, and after centrifugation, passed through a Ni column for affinity purification. The molecular size and purity of eluted protein was confirmed by SDS-PAGE. Production lot numbers and concentration information of the 20 Sarbecovirus proteins are shown in Supplementary Table 4. The WT RBD in the article is SARS-CoV-2 (2019-nCoV) Spike RBD-His Recombinant Protein (SinoBiological, 40592-V08H).

A panel of 21 sarbecovirus RBDs (Supplementary Table 3) in PBS was pre-coated onto ELISA Plates (NEST, 514201) at 4℃ overnight. The plates were washed and blocked. Then 1μg/ml purified antibodies or serially diluted antibodies were added and incubated at room temperature (RT) for 20min. Next, Peroxidase-conjugated AffiniPure Goat Anti-Human IgG (H+L) (JACKSON, 109-035-003) was applied and incubated at RT for 15min. Tetramethylbenzidine (TMB) (Solarbio, 54827-17-7) was added onto the plates. The reaction was terminated by 2 M H_2SO_4 after 10min incubation. Absorbance was measured at 450 nm using Ensight Multimode Plate Reader (PerkinElmer, HH3400). ELISA OD450 measurements at different antibody concentration for a particular antibody-antigen pair are fit to the model $y=Ac^n/(c^n + E^n)$ using R

package mosaic (v1.8.3), where y is OD450 values and c is corresponding antibody concentration. A, E, n are parameters, where E is the desired EC_{50} value for the specific antibody and antigen.

Antibody-ACE2 competition for RBD

Omicron-RBD (Sino Biological, 40592-V08H121) protein in PBS was immobilized on the ELISA plates at 4℃ overnight. The coating solution was removed and washed three times by PBST and the plates were then blocked for 2 h. After blocking, the plates were washed five times, and the mixture of ACE2-biotin (Sino Biological, 10108-H27B-B) and serially diluted competitor antibodies was added followed by 30min incubation at RT. Then Peroxidase-conjugated Streptavidin (Jackson ImmunoResearch, 016-030-084) was added into each well for another 20min incubation at RT. After washing the plates for five times, Tetramethylbenzidine (TMB) (Solarbio, 54827-17-7) was added into each well. After 10 min, the reaction was terminated by 2M H_2SO_4. Absorbance was measured at 450 nm using Ensight Multimode Plate Reader (PerkinElmer, HH3400). The ACE2 competition coefficient is calculated as (B-A)/B, where B is the OD450 value under 0.3ug/ml antibody concentration and A is the OD450 value under 6ug/ml antibody concentration.

Biolayer Interferometry

Biolayer interferometry assays were performed on Octet® RED 384 Protein Analysis System (Fortebio) according to the manufacturer's instruction. To measure the binding affinities, monoclonal antibodies were immobilized onto Protein A biosensors (Fortebio) and the fourfold serial dilutions of Omicron S trimer (BA.1 and BA.2) in PBS were used as analytes. Data were collected with Octet Acquisition 9.0 (Fortebio) and analyzed by Octet Analysis 9.0 (Fortebio) and Octet Analysis Studio 12.2 (Fortebio).

S trimer thermal stability assay

The thermal stability assay was performed to detect the exposed hydrophobic residues by an MX3005 qPCR instrument (Agilent, Santa Clara, USA) with SYPRO Red (Invitrogen, Carlsbad, USA) as fluorescent probes. Here, we set up 25 μL reaction system (pH=8.0) which contained 5 μg of target protein (S trimer of Omicron lineage), 1000x SYPRO Red, and ramped up the temperature from 25°C to 99°C. Fluorescence was recorded in triplicate at an interval of 1°C.

Surface plasmon resonance

Human ACE2 was immobilized onto CM5 sensor chips using a Biacore 8K (GE Healthcare). Serial dilutions of purified S trimer of Omicron lineages were injected, ranging in concentrations from 100 to 6.25 nM. The response units were recorded at room temperature and the resulting data were fitted to a 1:1 binding model using Biacore Evaluation Software (GE Healthcare).

Protein expression and purification for cryo-EM study

The S6P expression construct encoding the SARS-CoV-2 spike ectodomain (residues 1-1208) with six stabilizing Pro substitutions (F817P, A892P, A899P, A942P, K986P, and V987P) and a "GSAS" substitution for the furin cleavage site (residues 682–685) was previously described[15]. The Delta specific mutations (T19R, G142D, 156del, 157del, R158G, L452R, T478K, D614G, P681R, D950N) were introduced into this construct using site-directed mutagenesis. The S6P expression construct containing the Omicron BA.1 mutations (A67V, H69del, V70del, T95I, G142D, V143del, Y144del, Y145del, N211del, L212I, ins214EPE, G339D, S371L, S373P, S375F, K417N, N440K, G446S, S477N, T478K, E484A, Q493R, G496S, Q498R, N501Y, Y505H, T547K, D614G, H655Y, N679K, P681H, N764K, D796Y, N856K, Q954H, N969K, L981F) were assembled from three synthesized DNA fragments. The S6P expression construct containing the Omicron BA.2 mutations (T19I, L24S, del25-27, G142D, V213G, G339D, S371F, S373P, S375F, T376A, D405N, R408S, K417N, N440K, G446S, S477N, T478K, E484A, Q493R, Q498R, N501Y, Y505H, D614G, H655Y, N679K, P681H, N764K, D796Y, Q954H, N969K) were assembled from three synthesized DNA fragments. The expression constructs encoding the SARS-CoV spike ectodomain (residues 1-1195)[46] was kindly provided by Prof. X. Wang

(Tsinghua University), and two stabilizing Pro substitutions (K968P, V969P) was engineered into this construct using mutagenesis. For protein production, these expression plasmids, as well as the plasmids encoding the antigen-binding fragments (Fabs) of the antibodies described in this paper, were transfected into the HEK293F cells using polyethylenimine (Polysciences). The conditioned media were harvested and concentrated using a Hydrosart ultrafilter (Sartorius), and exchanged into the binding buffer (25 mM Tris, pH 8.0, and 200 mM NaCl). Protein purifications were performed using the Ni-NTA affinity method, followed by gel filtration chromatographies using either a Superose 6 increase column (for the spike proteins) or a Superose 200 increase column (for the Fabs). The final buffer used for all proteins is 20 mM HEPES, pH 7.2, and 150 mM NaCl.

Cryo-EM data collection, processing, and structure building

The samples for cryo-EM study were prepared essentially as previously described[15,47] (Supplementary Table 4). All EM grids were evacuated for 2 min and glow-discharged for 30 s using a plasma cleaner (Harrick PDC-32G-2). Four microliters of spike protein (0.8 mg/mL) was mixed with the same volume of Fabs (1 mg/mL each), and the mixture was immediately applied to glow-discharged holy-carbon gold grids (Quantifoil, R1.2/1.3) in an FEI Vitrobot IV (4 °C and 100% humidity). Data collection was performed using either a Titan Krios G3 equipped with a K3 direct detection camera, or a Titan Krios G2 with a K2 camera, both operating at 300 kV. Data processing was carried out using cryoSPARC[48]. After 2D classification, particles with good qualities were selected for global 3D reconstruction and then subjected to homogeneous refinement. To improve the density surrounding the RBD-Fab region, UCSF Chimera[49] and Relion[50] were used to generate the masks, and local refinement was then performed using cryoSPARC. Coot[51] and Phenix[52] were used for structural modeling and refinement. Figures were prepared using USCF ChimeraX[53] and Pymol (Schrödinger, LLC.).

Data availability

Processed mutation escape scores can be downloaded at https://github.com/jianfcpku/SARS-CoV-2-RBD-DMS-broad. Raw Illumina and PacBio sequencing data are available on NCBI Sequence

Read Archive BioProject PRJNA804413. We used vdj_GRCh38_alts_ensembl-5.0.0 as the reference of V(D)J alignment, which can be obtained from https://support.10xgenomics.com/single-cell-vdj/software/downloads/latest.

IMGT/DomainGapAlign is based on the built-in lastest IMGT antibody database, and we let the "Species" parameter as "Homo sapiens" while kept the others as default. Public deep mutational scanning datasets involved in the study from literature could be downloaded at https://media.githubusercontent.com/media/jbloomlab/SARS2_RBD_Ab_escape_maps/main/processed_data/escape_data.csv.

Cryo-EM density maps have been deposited in the Electron Microscopy Data Bank with accession codes EMD-33210, EMD-33211, EMD-33212, EMD-33213, EMD-33323, EMD-33324, EMD-33325, EMD-32732, EMD-32738, EMD-32734, EMD-32718, and EMD-33019, respectively. Structural coordinates have been deposited in the Protein Data Bank with accession codes 7XIW, 7XIX, 7XIY, 7XIZ, 7XNQ, 7XNR, 7XNS 7WRL, 7WRZ, 7WRO, 7WR8 and 7X6A.

Code availability

Python and R scripts for analyzing escaping mutation profile data and reproducing figures in this manuscript are available at https://github.com/jianfcpku/SARS-CoV-2-RBD-DMS-broad.

Ethical Statement

This study was approved by the Ethics Committee of Beijing Ditan Hospital affiliated to Capital Medical University (Ethics committee archiving No. LL-2021-024-02), the Tianjin Municipal Health Commission, and the Ethics Committee of Tianjin First Central Hospital (Ethics committee archiving No. 2022N045KY). Informed consent was obtained from all human research participants.

Acknowledgments

We thank J. Bloom for his gift of the yeast SARS-CoV-2 WT RBD libraries. We thank Sino Biological for the technical assistance on mAbs and RBD expression. We thank J. Luo and H. Lv

for the help with flow cytometry. This project is financially supported by the Ministry of Science and Technology of China (CPL-1233).

Author contributions

Y.C. and X.S.X designed the study. Y.C., F.J. and X.S.X wrote the manuscript with inputs from all authors. Y.C. and F.S. coordinated the expression and characterization of the neutralizing antibodies. J.W. (BIOPIC), F.J., L.Z., H.S. performed and analyzed the yeast display screening experiments. T.X., P.W., J.W. (Changping Laboratory), R.A., Y.W., J.Z., N.Z., R.W., X.N., L.Y., C.L., X. S. L.Z., F.S. performed the neutralizing antibody expression and characterization, including pseudovirus neutralization and ELISA. W.H., Q.L., Y.W. prepared the VSV-based SARS-CoV-2 pseudovirus. A.Y., Y.W., S.Y., R.A., W.S. performed and analyzed the antigen-specific single B cell VDJ sequencing. S.D., P.L., Z.Z., L.W., R.F., Z.L., X.W., J.X. performed the structural analyses. X.H., W.Z., D.Z., and R.J. recruited the SARS convalescents and SARS-CoV-2 vaccinees. X.C. and Z.S. recruited the Omicron BA.1 convalescents. Q.G. proofed the manuscript.

Competing interests

X.S.X. and Y.C. are inventors on the provisional patent applications of BD series antibodies, which includes BD30-604 (DXP-604), BD55-5840 (SA58) and BD55-5514 (SA55). X.S.X. and Y.C. are founders of Singlomics Biopharmaceuticals. Other authors declare no competing interests.

References

1 Chen, C. *et al.* CoV-Spectrum: analysis of globally shared SARS-CoV-2 data to identify and characterize new variants. *Bioinformatics* **38**, 1735-1737, doi:10.1093/bioinformatics/btab856 (2021).

2 Greaney, A. J. *et al.* Complete Mapping of Mutations to the SARS-CoV-2 Spike Receptor-Binding Domain that Escape Antibody Recognition. *Cell Host Microbe* **29**, 44-57 e49, doi:10.1016/j.chom.2020.11.007 (2021).

3 Cao, Y. *et al.* Omicron escapes the majority of existing SARS-CoV-2 neutralizing antibodies. *Nature* **602**, 657-663, doi:10.1038/s41586-021-04385-3 (2022).

4 Westendorf, K. *et al.* LY-CoV1404 (bebtelovimab) potently neutralizes SARS-CoV-2 variants. *bioRxiv*, 2021.2004.2030.442182, doi:10.1101/2021.04.30.442182 (2022).

5 Zost, S. J. *et al.* Potently neutralizing and protective human antibodies against SARS-CoV-2. *Nature* **584**, 443-449, doi:10.1038/s41586-020-2548-6 (2020).
6 Cele, S. *et al.* Omicron extensively but incompletely escapes Pfizer BNT162b2 neutralization. *Nature* **602**, 654-656, doi:10.1038/s41586-021-04387-1 (2022).
7 Collie, S., Champion, J., Moultrie, H., Bekker, L.-G. & Gray, G. Effectiveness of BNT162b2 Vaccine against Omicron Variant in South Africa. *New England Journal of Medicine* **386**, 494-496, doi:10.1056/NEJMc2119270 (2021).
8 Lu, L. *et al.* Neutralization of SARS-CoV-2 Omicron variant by sera from BNT162b2 or Coronavac vaccine recipients. *Clin Infect Dis*, ciab1041, doi:10.1093/cid/ciab1041 (2021).
9 Cameroni, E. *et al.* Broadly neutralizing antibodies overcome SARS-CoV-2 Omicron antigenic shift. *Nature* **602**, 664-670, doi:10.1038/s41586-021-04386-2 (2022).
10 Dejnirattisai, W. *et al.* SARS-CoV-2 Omicron-B.1.1.529 leads to widespread escape from neutralizing antibody responses. *Cell* **185**, 467-484 e415, doi:10.1016/j.cell.2021.12.046 (2022).
11 Liu, L. *et al.* Striking antibody evasion manifested by the Omicron variant of SARS-CoV-2. *Nature* **602**, 676-681, doi:10.1038/s41586-021-04388-0 (2022).
12 Planas, D. *et al.* Considerable escape of SARS-CoV-2 Omicron to antibody neutralization. *Nature* **602**, 671-675, doi:10.1038/s41586-021-04389-z (2022).
13 Bruel, T. *et al.* Serum neutralization of SARS-CoV-2 Omicron sublineages BA.1 and BA.2 in patients receiving monoclonal antibodies. *Nat Med*, doi:10.1038/s41591-022-01792-5 (2022).
14 Hsieh, C.-L. *et al.* Structure-based design of prefusion-stabilized SARS-CoV-2 spikes. *Science* **369**, 1501-1505, doi:doi:10.1126/science.abd0826 (2020).
15 Du, S. *et al.* Structurally Resolved SARS-CoV-2 Antibody Shows High Efficacy in Severely Infected Hamsters and Provides a Potent Cocktail Pairing Strategy. *Cell* **183**, 1013-1023 e1013, doi:10.1016/j.cell.2020.09.035 (2020).
16 Cui, Z. *et al.* Structural and functional characterizations of infectivity and immune evasion of SARS-CoV-2 Omicron. *Cell* **185**, 860-871 e813, doi:10.1016/j.cell.2022.01.019 (2022).
17 Starr, T. N. *et al.* Deep Mutational Scanning of SARS-CoV-2 Receptor Binding Domain Reveals Constraints on Folding and ACE2 Binding. *Cell* **182**, 1295-1310 e1220, doi:10.1016/j.cell.2020.08.012 (2020).
18 Iketani, S. *et al.* Antibody evasion properties of SARS-CoV-2 Omicron sublineages. *Nature*, doi:10.1038/s41586-022-04594-4 (2022).
19 Yamasoba, D. *et al.* Virological characteristics of SARS-CoV-2 BA.2 variant. *bioRxiv*, 2022.2002.2014.480335, doi:10.1101/2022.02.14.480335 (2022).
20 Tan, C. W. *et al.* Pan-Sarbecovirus Neutralizing Antibodies in BNT162b2-Immunized SARS-CoV-1 Survivors. *N Engl J Med* **385**, 1401-1406, doi:10.1056/NEJMoa2108453 (2021).
21 Hansen, J. *et al.* Studies in humanized mice and convalescent humans yield a SARS-CoV-2 antibody cocktail. *Science* **369**, 1010-1014, doi:10.1126/science.abd0827 (2020).
22 Shi, R. *et al.* A human neutralizing antibody targets the receptor-binding site of SARS-CoV-2. *Nature* **584**, 120-124, doi:10.1038/s41586-020-2381-y (2020).
23 Jones, B. E. *et al.* The neutralizing antibody, LY-CoV555, protects against SARS-CoV-2 infection in nonhuman primates. *Sci Transl Med* **13**, eabf1906, doi:10.1126/scitranslmed.abf1906 (2021).
24 Ju, B. *et al.* Human neutralizing antibodies elicited by SARS-CoV-2 infection. *Nature* **584**, 115-119, doi:10.1038/s41586-020-2380-z (2020).

25 Cao, Y. *et al.* Potent Neutralizing Antibodies against SARS-CoV-2 Identified by High-Throughput Single-Cell Sequencing of Convalescent Patients' B Cells. *Cell* **182**, 73-84 e16, doi:10.1016/j.cell.2020.05.025 (2020).
26 Rappazzo, C. G. *et al.* Broad and potent activity against SARS-like viruses by an engineered human monoclonal antibody. *Science* **371**, 823-829, doi:10.1126/science.abf4830 (2021).
27 Pinto, D. *et al.* Cross-neutralization of SARS-CoV-2 by a human monoclonal SARS-CoV antibody. *Nature* **583**, 290-295, doi:10.1038/s41586-020-2349-y (2020).
28 Park, Y. J. *et al.* Antibody-mediated broad sarbecovirus neutralization through ACE2 molecular mimicry. *Science* **375**, 449-454, doi:10.1126/science.abm8143 (2022).
29 Westendorf, K. *et al.* LY-CoV1404 (bebtelovimab) potently neutralizes SARS-CoV-2 variants. *bioRxiv*, 2021.2004.2030.442182, doi:10.1101/2021.04.30.442182 (2022).
30 Cao, Y. *et al.* Humoral immune response to circulating SARS-CoV-2 variants elicited by inactivated and RBD-subunit vaccines. *Cell Res* **31**, 732-741, doi:10.1038/s41422-021-00514-9 (2021).
31 Starr, T. N. *et al.* SARS-CoV-2 RBD antibodies that maximize breadth and resistance to escape. *Nature*, doi:10.1038/s41586-021-03807-6 (2021).
32 Greaney, A. J. *et al.* Mapping mutations to the SARS-CoV-2 RBD that escape binding by different classes of antibodies. *Nature Communications* **12**, 4196, doi:10.1038/s41467-021-24435-8 (2021).
33 Corti, D., Purcell, L. A., Snell, G. & Veesler, D. Tackling COVID-19 with neutralizing monoclonal antibodies. *Cell* **184**, 3086-3108, doi:10.1016/j.cell.2021.05.005 (2021).
34 Dejnirattisai, W. *et al.* The antigenic anatomy of SARS-CoV-2 receptor binding domain. *Cell* **184**, 2183-2200 e2122, doi:10.1016/j.cell.2021.02.032 (2021).
35 Piccoli, L. *et al.* Mapping Neutralizing and Immunodominant Sites on the SARS-CoV-2 Spike Receptor-Binding Domain by Structure-Guided High-Resolution Serology. *Cell* **183**, 1024-1042 e1021, doi:10.1016/j.cell.2020.09.037 (2020).
36 Barnes, C. O. *et al.* SARS-CoV-2 neutralizing antibody structures inform therapeutic strategies. *Nature* **588**, 682-687, doi:10.1038/s41586-020-2852-1 (2020).
37 Yuan, M. *et al.* Structural and functional ramifications of antigenic drift in recent SARS-CoV-2 variants. *Science* **373**, 818-823, doi:10.1126/science.abh1139 (2021).
38 Muecksch, F. *et al.* Increased Memory B Cell Potency and Breadth After a SARS-CoV-2 mRNA Boost. *Nature*, doi:10.1038/s41586-022-04778-y (2022).
39 Cao, Y. *et al.* Humoral immunogenicity and reactogenicity of CoronaVac or ZF2001 booster after two doses of inactivated vaccine. *Cell Research* **32**, 107-109, doi:10.1038/s41422-021-00596-5 (2022).
40 Zheng, H. *et al.* Disease profile and plasma neutralizing activity of post-vaccination Omicron BA.1 infection in Tianjin, China: a retrospective study. *medRxiv*, 2022.2004.2009.22273653, doi:10.1101/2022.04.09.22273653 (2022).
41 Hao, Y. *et al.* Integrated analysis of multimodal single-cell data. *Cell* **184**, 3573-3587 e3529, doi:10.1016/j.cell.2021.04.048 (2021).
42 Aran, D. *et al.* Reference-based analysis of lung single-cell sequencing reveals a transitional profibrotic macrophage. *Nature Immunology* **20**, 163-172, doi:10.1038/s41590-018-0276-y (2019).
43 Monaco, G. *et al.* RNA-Seq Signatures Normalized by mRNA Abundance Allow Absolute Deconvolution of Human Immune Cell Types. *Cell Reports* **26**, 1627-1640.e1627, doi:https://doi.org/10.1016/j.celrep.2019.01.041 (2019).

44 Ehrenmann, F. & Lefranc, M. P. IMGT/DomainGapAlign: IMGT standardized analysis of amino acid sequences of variable, constant, and groove domains (IG, TR, MH, IgSF, MhSF). *Cold Spring Harb Protoc* **2011**, 737-749, doi:10.1101/pdb.prot5636 (2011).

45 Starr, T. N. *et al.* Shifting mutational constraints in the SARS-CoV-2 receptor-binding domain during viral evolution. *bioRxiv*, 2022.2002.2024.481899, doi:10.1101/2022.02.24.481899 (2022).

46 Gui, M. *et al.* Cryo-electron microscopy structures of the SARS-CoV spike glycoprotein reveal a prerequisite conformational state for receptor binding. *Cell Res* **27**, 119-129, doi:10.1038/cr.2016.152 (2017).

47 Du, S. *et al.* Structures of SARS-CoV-2 B.1.351 neutralizing antibodies provide insights into cocktail design against concerning variants. *Cell Res* **31**, 1130-1133, doi:10.1038/s41422-021-00555-0 (2021).

48 Punjani, A., Rubinstein, J. L., Fleet, D. J. & Brubaker, M. A. cryoSPARC: algorithms for rapid unsupervised cryo-EM structure determination. *Nat Methods* **14**, 290-296, doi:10.1038/nmeth.4169 (2017).

49 Pettersen, E. F. *et al.* UCSF Chimera--a visualization system for exploratory research and analysis. *J Comput Chem* **25**, 1605-1612, doi:10.1002/jcc.20084 (2004).

50 Zivanov, J. *et al.* New tools for automated high-resolution cryo-EM structure determination in RELION-3. *Elife* **7**, doi:10.7554/eLife.42166 (2018).

51 Emsley, P., Lohkamp, B., Scott, W. G. & Cowtan, K. Features and development of Coot. *Acta crystallographica. Section D, Biological crystallography* **66**, 486-501, doi:10.1107/S0907444910007493 (2010).

52 Liebschner, D. *et al.* Macromolecular structure determination using X-rays, neutrons and electrons: recent developments in Phenix. *Acta Crystallogr D Struct Biol* **75**, 861-877, doi:10.1107/S2059798319011471 (2019).

53 Pettersen, E. F. *et al.* UCSF ChimeraX: Structure visualization for researchers, educators, and developers. *Protein Sci* **30**, 70-82, doi:10.1002/pro.3943 (2021).

Supplementary Files

This is a list of supplementary files associated with this preprint. Click to download.

- SIGuide.docx
- SupplementaryTable1.xlsx
- SupplementaryTable3.xlsx
- SupplementaryTable4.xlsx
- SupplementaryTable2.xlsx